

LoL-PIM: Long-Context LLM Decoding with Scalable DRAM-PIM System

Hyucksung Kwon* Kyungmo Koo* Janghyeon Kim Woongkyu Lee Minjae Lee
Hyungdeok Lee† Yousub Jung† Jaehan Park† Yosub Song† Byeongsu Yang†
Haerang Choi† Guhyun Kim† Jongsoon Won† Woojae Shin† Changhyun Kim†
Gyeongcheol Shin† Yongkee Kwon† Ilkon Kim† Euicheol Lim†
John Kim§ Jungwook Choi

Hanyang University, †Solution Advanced Technology, SK hynix, §KAIST

ABSTRACT

The expansion of large language models (LLMs) with hundreds of billions of parameters presents significant challenges to computational resources, particularly data movement and memory bandwidth. *Long-context* LLMs, which process sequences of tens of thousands of tokens, further increase the demand on the memory system as the complexity in attention layers and key-value cache sizes is proportional to the context length. Processing-in-Memory (PIM) maximizes memory bandwidth by moving compute to the data and can address the memory bandwidth challenges; however, PIM is not necessarily scalable to accelerate long-context LLM because of limited per-module memory capacity and the inflexibility of fixed-functional unit PIM architecture and *static* memory management. In this work, we propose LoL-PIM— a multi-node PIM architecture that accelerates long context LLM through hardware-software co-design. In particular, we propose how pipeline parallelism can be exploited across a multi-PIM module while a direct PIM access (DPA) controller (or DMA for PIM) is proposed that enables dynamic PIM memory management and results in efficient PIM utilization across a diverse range of context length. We developed an MLIR-based compiler for LoL-PIM— a commercial PIM-based compiler where the software modifications were implemented and evaluated, while the hardware changes were modeled in the simulator. Our evaluations demonstrate that LoL-PIM significantly improves throughput and reduces latency for long-context LLM inference, outperforming both multi-GPU and GPU-PIM systems (up to 8.54× and 16.0× speedup, respectively), thereby enabling more efficient deployment of LLMs in real-world applications.

1 INTRODUCTION

The rapid advancement of large language models (LLMs) has transformed fields ranging from natural language processing to intelligent agents by enabling the generation of contextually relevant responses across diverse applications [11, 25, 53, 61, 63]. In particular, *long-context* LLMs, capable of maintaining coherence across tens of thousands of tokens, have significantly enhanced contextual relevance in various tasks. For instance, long document summarization [73] generates cohesive summaries from dispersed information across different sections of extensive text, while repository-level code analysis [45] extends programming assistants’ capabilities to analyze entire codebases comprising thousands of lines. Furthermore, chain-of-thought

(CoT) reasoning has recently improved answer quality by leveraging multi-step contextual reasoning [52, 67]. These advancements rely on inference-time processing of extended contexts, with recent LLMs supporting long-context handling capabilities ranging from 16K to 200K tokens [7, 11, 48, 52].

There have been many recent works on accelerating LLM inference, but most have focused on LLM inferences with shorter context (i.e., up to 4 or 8k) [5, 21, 69, 72]. As the context length increases, both the memory capacity and the memory bandwidth become a greater bottleneck during LLM inference. In particular, the memory capacity for the key-value cache (KV-cache), which is needed during Attention computation, increases linearly with the input context length. Since Attention relies on general matrix-vector multiplication (GEMV), the compute density (operations per byte) of LLM decoding is reduced and decoding becomes memory bandwidth bound. To provide sufficient memory capacity and bandwidth, multi-GPUs are commonly used but results in underutilization of GPU compute.

To address the memory bandwidth challenges, DRAM-based Processing-in-Memory (PIM) technology offers a promising solution by embedding computational capabilities directly within the memory [6, 10, 19, 32, 38, 40, 49, 54]. Fixed-functional unit PIM systems, such as AiMX [18, 32, 34, 35, 41], are particularly well-suited for accelerating GEMV in LLM inference by exploiting the high internal memory bandwidth within DRAM modules. While PIM can accelerate GEMV, leveraging PIM for long-context LLM decoding presents new challenges, including the following.

- (1) **Memory capacity:** Individual PIM chip memory capacity is limited to a few GBs and is problematic for large KV-caches that require up to hundreds of GBs for long context.
- (2) **Static PIM memory management:** Long-context LLM have a diverse set of input context lengths and a fixed (or static) memory management results in inefficient usage of PIM memory and reduces overall throughput.
- (3) **I/O buffer bottleneck:** Non-square, aspect ratio of KV-cache, caused by long context inputs, creates a new PIM bottleneck in the I/O buffers.

Recent work [19, 54, 57] exploit PIM and heterogeneous architectures (e.g., GPU-PIM or NPU-PIM) to accelerate LLM inference; however, they focus on short-context LLM (under 2k tokens) and do not address the challenges of long-context LLM. In particular, prior work often have assumed fixed context length when serving multiple requests; however, making the same assumption for long-context

*Equal contribution.

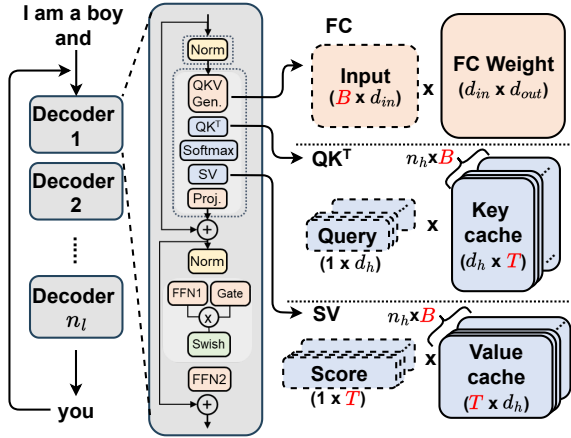


Figure 1: Decoding Computation for Long-Context LLM.

LLM results in poor utilization of the PIM since PIM memory would need to be allocated for the maximum context length, which can be an order of magnitude higher than the average context length. To overcome the challenges of accelerating long-context LLM, this work proposes LoL-PIM, a novel scalable multi-node PIM system architecture for long-context LLM that supports up to 32K tokens. Each node in LoL-PIM consists of multiple PIM modules to provide sufficient memory capacity (and bandwidth) to address the challenges of long-context LLM acceleration. *PIM-aware* partitioning of the KV-cache and weight matrix is proposed to enable sequence parallelism within the PIM modules to maximize bandwidth utilization and improve decoding throughput (tokens/sec).

Modern PIM [34, 40] architectures with fixed-functional units are often restricted to *static* PIM memory management because of limited programmability. This is problematic for long-context LLM since each request must be allocated based on the *maximum* context length. To address this limitation, LoL-PIM proposes *dynamic* memory management through Direct PIM Access (DPA) controller, or DMA for PIM, to support diverse KV-cache sizes and enable “lazy” PIM memory allocation. This results in efficient usage of PIM memory capacity for long-context LLM while also supporting larger batch sizes to improve overall throughput. Both PIM-aware data partitioning and dynamic memory management maximize internal memory bandwidth and ensure efficient utilization of PIM memory but create a new bottleneck in the PIM I/O. Thus, LoL-PIM includes a novel PIM I/O-aware buffering to mitigate the I/O bottleneck in long-context LLM. In particular, *ping-pong* I/O buffer is proposed which double buffers PIM input and output to overlap I/O data movement with PIM computation.

We evaluate LoL-PIM’s scalable decoding performance on popular long-context LLMs (7B to 72B parameters) using long-context tasks (token length ranging from 2K to 32K) from a representative benchmark, LongBench [8]. We evaluate LoL-PIM as both PIM-only system or a heterogeneous system with a GPU. Our evaluations show

LoL-PIM outperforms the baseline GPU and the commercial AiMX in token generation throughput by 8.54× and 4.74×.

Model	n_l	n_h	d_h	SwiGLU	GQA	Reference	CTL
LLM-1.8B	24	16	64	✓	×	Qwen1.5-1.8B [7]	32K
LLM-7B	32	32	128	× (ReLU)	×	MPT-7B-story [48]	65K
				✓	×	Qwen1.5-7B [7]	32K
LLM-14B	40	40	128	✓	✓	Llama3.1-8B [14]	128K
				✓	×	Qwen1.5-14B [7]	32K
LLM-72B	80	64	128	✓	✓	LongChat-13B [43]	16K
				✓	×	Qwen1.5-72B [7]	32K
				✓	✓	Llama3.1-70B [14]	128K

Table 1: Specifications and context length(CTL) limits of various Long-Context LLMs.

Task	QMSum	HotpotQA	Musique
mean	13966	13465	16362
std	6182	3921	1651
max	30456	17674	17917
min	2651	1917	6820

Table 2: Statistics of input context length with tokenizer of Qwen Model (LongBench [8]).

2 BACKGROUND

2.1 Long-context LLM Decoding

Long-context LLM Inference. Long-context LLMs excel at maintaining coherence over tens of thousands of tokens, significantly enhancing contextual relevance across various tasks – e.g., long document summarization [73] generates cohesive summaries from information spread across different sections of extensive text, and repository-level code analysis [45] extends programming assistants’ capabilities to analyze entire codebases comprising thousands of lines. Chain-of-thought (CoT) reasoning also improves answer quality by leveraging multi-step contextual reasoning [52, 67]. These advancements rely on inference-time processing of extended contexts, with modern LLMs supporting token lengths ranging from 16K to 200K [7, 11, 48, 52]. Table 1 summarizes publicly available long-context LLMs, including the number of layers (n_l), attention heads (n_h), and the feature dimension of each head (d_h), as well as structural variations like group query attention (GQA)[4] and SwiGLU[58]. (Implementation details are discussed in Sec.7). These models are trained on long-context datasets, enabling them to perform tasks requiring extended input contexts processing. Table 2 highlights the characteristics of popular long-context benchmarks, which exhibit significant variability in context lengths across requests.

Decoding Computation. Long-context large language models (LLMs) are constructed based on the Transformer decoder [64]. As illustrated in Fig. 1, each decoder of n_l layers comprises Multi-Head Attention (MHA) and Feed-Forward Network (FFN). Each head h of MHA starts with the Query/Key/Value generation (QKV-Gen) that generates vectors $\{Q, K, V\} \in \mathbb{R}^{d_h}$, where K and V are stacked to KV-cache $\in \mathbb{R}^{t \times d_h}$ for t tokens. It is followed by the score generation (QK^T), which is then scaled and softmaxed ($S = \text{softmax}(QK^T \sqrt{d_h})$) to generate the scaled-dot-product attention (SV). Then, SV concatenated across n_h heads is projected (Proj) to become the MHA output. FFN consists of two consecutive fully-connected (FC) layers, FFN1 and FFN2, with an activation function in between for non-linear transformation. In sum, the Transformer decoder computation can be categorized into two types: FC-layers (QKV-Gen, Proj, FFN1, FFN2) that involve weight matrix, and attention-layers (QK^T and SV) that involve KV-cache.

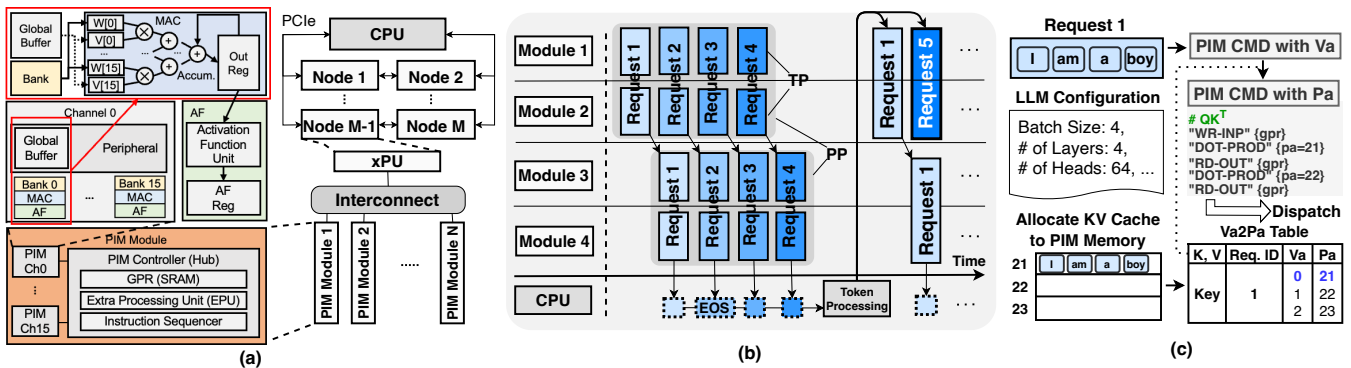


Figure 2: Multi-node PIM system and parallel LLM execution. (a) A multi-node PIM system organization. (b) A tensor parallel (TP) and pipeline parallel (PP) LLM execution. (c) The execution flow of PIM commands for LLM inference.

PIM Cmd	Description	Arguments	Ref. Cmd [32]
WR-INP	Copy Input from GPR to GB	GPR index	WRGB
DOT-PROD	Dot-Product on a DRAM row	Row/Col index	MACABK
RD-OUT	Copy Output from OutReg to GPR	GPR index	RDMAC

Table 3: PIM commands for mapping LLM inference.

2.2 Multi-node Domain-specific PIM System

DRAM-based Domain-specific PIM. DRAM-based Processing-in-Memory (PIM) technology addresses memory-bound challenges by integrating computational capabilities directly within the memory subsystem [6, 10, 19, 32, 38, 40, 49, 54]. Fixed functional unit PIM systems are optimized for accelerating LLM inference through GEMV operations. These PIM feature processing units adjacent to DRAM banks for parallel dot-product computations, pre-generated PIM commands for simplified control, and limited conditional logic to minimize area overhead [18, 32, 34, 35, 41]. For example, AiMX [18, 32, 34, 35, 41] includes a vector multiply-accumulate unit in each DRAM bank for 16-element dot-product computations, a shared 2KB global buffer for input data, and a minimal pair of 2-byte output registers per processing unit to transfer results off-chip for module-level processing (e.g., Softmax) using Extra Processing Unit (Fig. 2(a)). Additionally, all channels share a broadcasting input data path to minimize resource usage.

Multi-node PIM System. Fig. 2 (a) illustrates the LLM inference on a multi-node system. The system consists of a host CPU connected with multiple nodes, each consisting of a compute-intensive xPU (i.e., GPU or NPU) connected with multiple PIM modules that provide extensive internal memory bandwidth. As motivated by prior works [19, 54, 57], xPU takes responsibility for the compute-intensive context summarization phase (prefill), while PIM modules handle the memory-bandwidth/capacity-demanding token generation phase (decoding). PIM Controller supports program execution for LLM inference compiled for model-parallel serving. Tensor-parallel (TP) processing [59] performs head-wise partitioning of MHA and FFN computations to minimize synchronization, while pipelined parallelism (PP) [22, 46] groups the layers and assigns a node to each layer-group for batch-wise parallel processing. As an example, Fig. 2(b) illustrates a parallel execution of four inference requests in a batch are partitioned over four PIM modules (i.e., $(TP, PP) = (2, 2)$), being dynamically managed as the request (= Request1) with the

end-of-sequence (EOS) token is replaced with a new request (= Request5).

Execution Flow. Executing LLM inference on PIM hardware involves generating PIM commands (Table 3) to manage tasks such as matrix multiplications and attention mechanisms. Fig. 2(c) illustrates the execution flow, where the PIM module interacts with DRAM to store KV caches and directly compute dot-products. These PIM commands incorporate key configuration details such as layers, attention heads, and batch size. However, since the number of tokens during inference is unknown at compile time, PIM commands must be pre-generated for all potential token ranges up to the maximum size, and memory must be pre-allocated accordingly.

3 MOTIVATION

3.1 Characteristics of Long-context LLM

Long-context LLM inference presents significant challenges due to the memory-intensive demands of Attention layers, particularly during token generation for batches of tens to hundreds of requests in the decoding phase. To analyze workload characteristics, we evaluate a long-context LLM (Qwen1.5-7B) on an A100-80GB GPU with input context lengths (L_{in}) ranging from 4K to 32K tokens. Weak scaling is used – thus, as the number of GPUs is scaled to ensure sufficient memory capacity, the batch size is maximized based on total GPU memory. The key observations are as follows:

- **KV-cache Memory Dominance:** The KV-cache consumes a far greater portion of memory compared to weight parameters, as its size is proportional to the context length. Each token generation requires a prefilled KV-cache for Attention computations, leading to significant memory usage as the context length increases (Fig. 3(a)).
- **Attention Bottleneck:** The growing computational demands of Attention become the major bottleneck at longer context lengths. Attention computations rely on general matrix-vector multiplication (GEMV), which reduces compute density (operations per byte) and makes decoding heavily reliant on memory bandwidth. While batch processing enhances throughput for fully connected (FC) layers, which use general matrix-matrix multiplication (GEMM), it exacerbates bandwidth limitations for Attention layers (Fig. 3(b)).

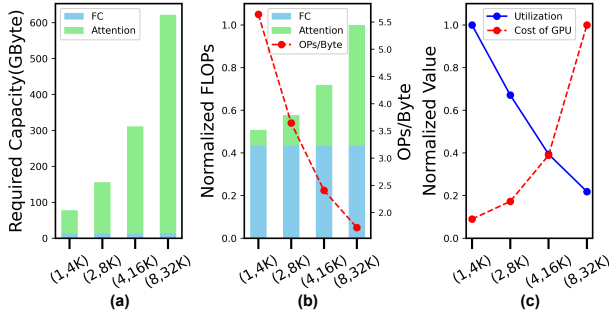


Figure 3: Characteristics of LLM workloads with scaling context length. The x-axis represents the number of GPUs and input context lengths (L_{in}). (a) Required memory capacity. (b) Floating-point operations and Ops/Byte. (c) GPU utilization and cost, normalized across configurations.

- **GPU Scalability:** A single GPU lacks the memory capacity and bandwidth required to support long-context LLM demands [3, 44, 56, 66, 68]. Multi-GPU can provide memory capacity and bandwidth but it results in underutilized computational resources and increased inference costs (tokens per dollar) that scale linearly with the number of GPU nodes (Fig. 3(c)).

3.2 Challenges of PIM Scaling

In this subsection, we highlight the challenges of scaling fixed-functional unit PIM architecture for long-context LLM decoding. First, bank-parallel dot-product efficiency of PIM relies on matrix partitioning, but KV-caches may exceed the capacity of a single PIM module. Increasing the number of PIM modules to accommodate longer contexts raises TP , distorting the partitioned subsection’s aspect ratio and incurring frequent input/output transfers that lead to I/O transfer overhead. Fig. 4(a) illustrates the scaling of context length and node count. In GPU systems, throughput suffers from low compute utilization caused by memory bottlenecks. While PIM improves throughput in LLM decoding, its effectiveness diminishes as TP -only parallelization limits scaling. This work identifies inefficiencies in PP from existing partitioning approaches and introduces a new strategy that enhances bank-parallel computation by enabling PP -friendly partitioning (Sec. 4).

Second, varying context lengths in decoding requests require *dynamic* PIM memory management, but fixed-functional PIM units have limited conditional control to maximize compute density. Commercial PIM with fixed-functional units are managed by pre-generated commands with embedded operand addresses, forcing memory allocation based on the maximum context length regardless of actual context length, leading to underutilized memory and constrained batch sizes. Fig. 4(b) demonstrates slow batch size growth in PIM systems. To address this, we propose a dynamic memory management method using lightweight dynamic control commands for lazy memory allocation, significantly increasing average batch size. As shown in Fig. 4(b), the proposed method achieves near-ideal batch sizes (Sec. 5).

Third, the KV-cache’s structure suffers from distortion due to low d_h , while the aspect ratio of weight parameters becomes increasingly

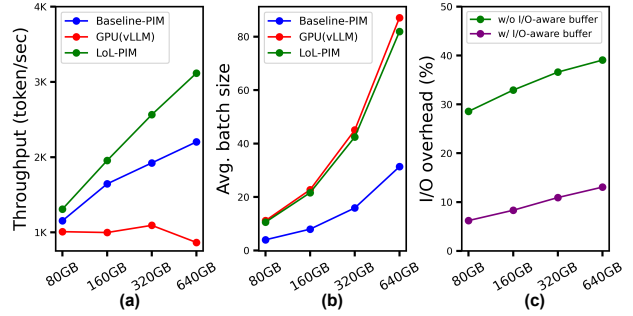


Figure 4: Performance evaluation of the proposed LoL-PIM compared to baseline-PIM and GPU implementations. The x-axis represents the system’s memory capacity, and the workload (context length: L_{in}) assigned to each case increases proportionally with the system’s capacity, like Fig. 3 (Capacity = 80GB \times N, Context length = 4K \times N).

biased as more PIM modules partition them. This biased matrix aspect ratio limits input and output reuse. Fixed-functional PIMs exacerbate this by constraining data transfer paths, resulting in significant I/O overhead. To mitigate this, we propose an I/O-aware buffering mechanism that overlaps data transfer with PIM computation. The resource overhead is minimal, as channels or banks share the buffers. Fig. 4(c) shows a substantial reduction in I/O overhead across varying context lengths (Sec. 6).

4 SCALABLE PIM ARCHITECTURE

4.1 PIM-aware Partitioning

LLM decoding workloads rely on weight parameter matrices and the KV-cache. Workload partitioning ensures that the dimensions of the matrix are distributed across PIM modules, with each subsection fitting within the memory capacity of the module: $N_{ch} \cdot N_{bank} \times D_{row} \cdot N_{row}$. When partitioning LLM workloads across multiple PIM modules, two primary parallelization methods are used: Pipeline Parallelization (PP) [22, 46], which groups LLM layers into PP pipeline stages, and Tensor Parallelization (TP) [59], which divides matrix dimensions within each group by TP . While both approaches are widely applied in LLM inference systems, TP is more commonly preferred in multi-node PIM systems. A widely used strategy in prior works, called head-first allocation (HFA) [19, 54, 57], is summarized below (Fig. 5(a)):

- **Partitioning Weight Parameters.** In FC layers, weight parameters are typically partitioned by TP : d_{out} for QKV and $FFN1$, and d_{in} for $Proj$ and $FFN2$, as per Tensor Parallelization [59].
- **Partitioning KV-cache.** In Attention computation, the dimensions n_h and B are independent and parallelized by TP , ensuring each request’s per-head KV-cache resides within a single channel [19, 54].

Increasing the number of PIM modules to support longer contexts raises TP , but this approach introduces inefficiencies (Fig. 5(a)): 1) In FC layers, excessive TP distorts the partitioned subsection’s aspect ratio, causing frequent input/output transfers and resulting in I/O overhead. 2) In Attention layers, increasing TP reduces channel occupancy, leading to bank underutilization.

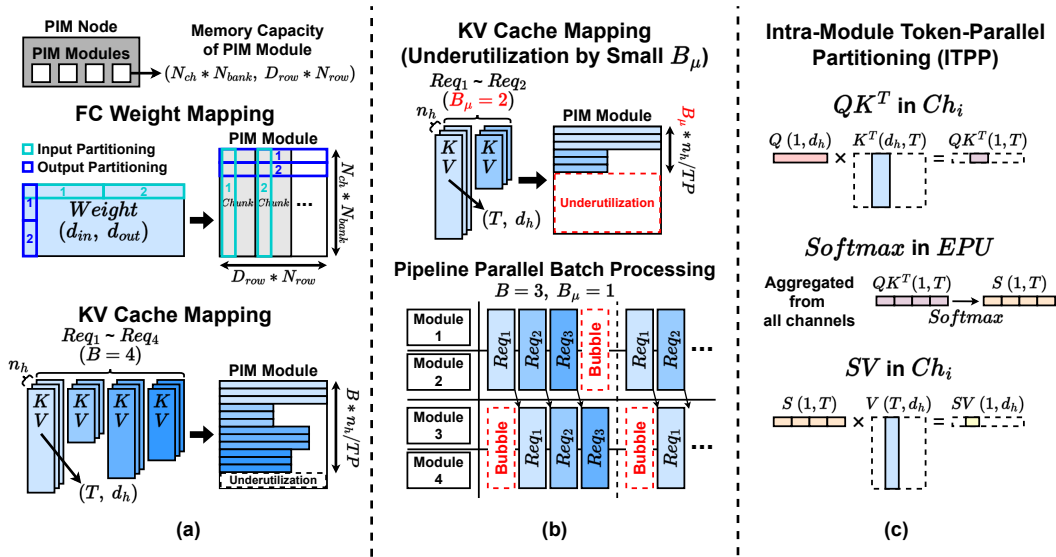


Figure 5: (a) PIM-aware partitioning. (b) Challenges for PIM-based pipeline parallelization. (c) Intra-module token-parallel partitioning.

4.2 Challenges for PIM-based Pipeline Parallelization

As the number of PIM modules increases, *PP* becomes essential to address inefficiencies in bandwidth utilization caused by overly aggressive *TP*. However, using *PP* with the HFA partitioning method presents a challenging performance trade-off. As shown in Fig. 5(b), each PIM module processes a micro-batch (B_μ) of the KV-cache during Attention computation. For a given batch size B , determined by the memory capacity for static max-context-length allocation, the number of batch processing steps is B/B_μ .

Pipeline bubbles, caused by host-PIM synchronization, grow as B_μ increases, leading to significant overhead. Conversely, smaller B_μ values result in fewer banks being used for parallel processing, causing underutilization. This trade-off has made *PP* less favorable in multi-PIM parallelization, as noted in [19].

4.3 Intra-module Token-parallel Partitioning

Achieving balanced channel utilization requires minimizing batch dimension partitioning during KV-cache allocation. To address this, we propose a new strategy called intra-module token-parallel partitioning (ITPP). As shown in Fig. 5(c), this approach prioritizes the partitioning of output dimensions over the batch dimension, allocating the KV-cache based on their respective output dimensions: the token dimension for the Key cache and the head dimension for the Value cache.

ITPP differs from prior strategies in two key ways. First, it allocates the token dimension for bank-level parallelization, leveraging the abundant token dimension in long-context LLM workloads to avoid bank underutilization. Unlike HFA, which over-partitions the batch dimension and suffers from *PP* trade-offs, ITPP ensures more efficient utilization. Second, ITPP aggregates token-parallel outputs of QK^T within a module, enabling the Extra Processing Unit (EPU) in the PIM Controller Hub to compute the Softmax aggregation.

This allows for head-wise pipelined execution of the Softmax and subsequent *SV* computation without incurring additional overhead. In contrast, Flash-Decoding [12, 20] involves numerically unstable partial Softmax computation [15] and costly inter-module communication. By combining the parallel computation advantages of Flash-Decoding for QK^T and the effective *SV* handling of HFA, ITPP delivers the best of both approaches. In summary, the benefits of the ITPP strategy include the following:

- **Balancing KV-cache Distribution.** HFA causes an imbalanced KV-cache distribution for storing long-context KV cache, leaving some channels within a PIM module idle while overloading others, which underutilizes bandwidth. In contrast, ITPP uses token-parallel partitioning to evenly distribute workloads, mitigate the effects of context-length variability, and minimize channel imbalances.
- **Consistent Channel Utilization.** By avoiding excessive partitioning of the batch dimension via token-parallel, ITPP ensures consistent utilization of all channels, even in cases with small batch sizes. By integrating output dimension prioritization and token dimension partitioning, LoL-PIM achieves efficient intra-module workload distribution without introducing additional overhead to attention operations.
- **Improved Bandwidth Utilization for FC-Layers.** ITPP enhances bandwidth utilization for FC layers by enabling pipeline parallelism (*PP*) in combination with tensor parallelism (*TP*), reducing excessive *TP* workload division.

5 DYNAMIC PIM MEMORY MANAGEMENT

Managing memory in long-context LLM decoding is challenging due to variability in context lengths. Although GPU-based approaches [13] have implemented dynamic memory allocation for such variability, PIM’s static control capabilities limit its adaptability. To overcome this, we introduce the Direct PIM Access (DPA)

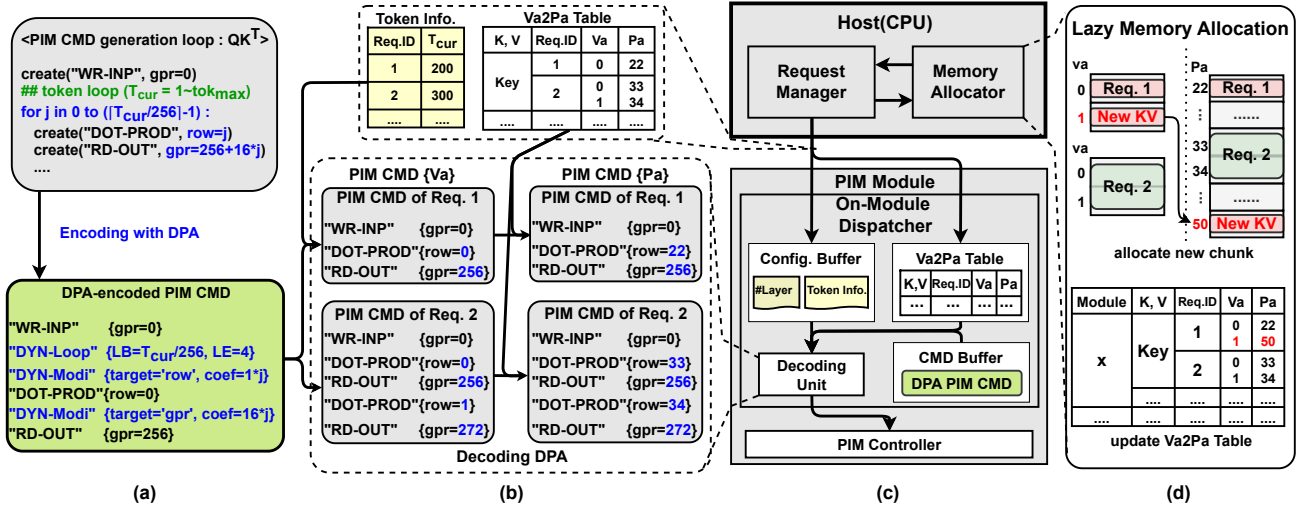


Figure 6: Direct PIM Access (DPA) controller. (a) DPA-encoded PIM commands. (b) DPA decoding example. (c) On-module dispatcher for supporting DPA. (d) Lazy memory allocation.

DPA Cmd.	Arguments	Description
Dyn-Loop	Loop-Bound (LB)	Num. PIM CMD repetition.
	Loop-Entry (LE)	Num. PIM commands that will be repeated
Dyn-Modi	Target	Target bit-field to adjust (eg. Row address)
	Coefficient	Value to modify target field

Table 4: Direct PIM Access (DPA) Commands.

controller, or DMA for PIM, which supports diverse KV-cache sizes and enables “lazy” memory allocation. DPA employs a lightweight set of commands and a command dispatching logic to facilitate dynamic memory management, significantly improving throughput in long-context LLM decoding.

5.1 Managing KV-cache in PIM

PIM accelerates Attention computations by managing the KV-cache within its memory modules. Recent studies [19, 54, 57] have used static memory allocation for the KV-cache, based on the *maximum* token length, and pre-generated PIM commands with fixed physical addresses (e.g., DOT-PROD(row,col) in Table 3). However, PIM lacks flow control instructions, requiring the compiler to pre-generate commands for all possible token lengths and select the appropriate one at runtime. This approach results in inefficient static memory allocation and token-length-agnostic command generation. Pre-generated commands with fixed operand indices cannot adapt to varying KV-cache sizes encountered during LLM decoding. To address these issues, we make two key observations:

- **Repetitive Compute Patterns:** The computation sequence for Attention operations (e.g., QK^T , SV) follows a *repetitive pattern* across layers and tokens. As shown in Fig. 6(a), the sequence consists of identical PIM commands, differing only in the number of repetitions (e.g., repeated DOT-PROD and RD-OUT commands as token length increases). This suggests the possibility of

dynamically unrolling PIM commands by encoding the repetition count.

- **Token-length-dependent Operands:** Operand indices for PIM commands are determined solely by token length. For example, DOT-PROD operand indices (row) are calculated as $row = T_{cur}/256$, derived from matrix partitioning. The Va2Pa table provides a one-to-one mapping between virtual addresses (Va) and physical addresses (Pa), enabling dynamic identification of the KV-cache data address. Virtual addresses (Va) are assigned logically and continuously, starting from 0 and incrementing by 1 for each data entry. For instance, in Request 1, $Va=0$ maps to $Pa=22$, while in Request 2, $Va=0$ maps to $Pa=33$. By using the physical address from this mapping, the KV-cache data address (e.g., row=22 or row=33) can be efficiently identified on-the-fly. Building on these insights, we propose a *DPA commands* to encode both repetition counts and operand modifications into a compact PIM command stack. This enables dynamic adjustment of PIM physical addresses to allocate and access KV-cache with varying context lengths during runtime. To implement this, we introduce a new PIM command set that includes *repetition counts* and *operand updates*. Additionally, we enhance the PIM module’s instruction dispatching logic to decode these commands and dynamically generate sequences at runtime. Together, these innovations provide a scalable and efficient solution for managing KV-cache in PIM environments, effectively addressing challenges posed by dynamic context lengths.

5.2 Direct PIM Access (DPA) Commands

Table 4 outlines the DPA commands designed to enhance the flexibility of PIM commands. These commands encapsulate repetitive token operations, enabling runtime execution without requiring re-compilation. The *Dyn-Loop* command encodes a loop structure, with Loop-Bound (LB) specifying the number of repetitions and Loop-Entry (LE) defining the number of commands to repeat. These parameters are determined dynamically based on the token length

of each request. The *Dyn-Modi* command adjusts target operand fields (e.g., Target=row for DOT-PROD) of the subsequent PIM command using a coefficient as the stride (e.g., Coef=1 for row-wise traversal of DOT-PROD). These modified operands function as virtual addresses, initialized at zero and incremented by the stride during runtime dispatch. The request ID and virtual address are then used to retrieve the corresponding physical address from the virtual-to-physical memory table. For example, as shown in Fig. 6(c), for Request-2 with $T_{cur} = 300$, LB=2 and LE=4. The first DOT-PROD command maps to the physical address (row=33), and the second maps to (row=34). This demonstrates how PIM commands dynamically determine operand physical addresses during runtime execution.

5.3 On-module PIM Command Dispatcher

To support DPA, we enhance the Instruction Sequencer within the PIM Controller (Fig. 2) to enable runtime dispatching of PIM commands. The on-module dispatcher manages dynamic command generation and memory allocation locally within the PIM module. Fig. 6(c) illustrates its components and operation, which include a Configuration Buffer, a Virtual-to-Physical Address (Va2Pa) Table, a Command Buffer, and a Decoding Unit. The total buffer size required for the dispatcher is minimal, less than 200KB (Table 5, which is significantly smaller than the 512KB GPR capacity in typical PIM Control Hubs [70], ensuring efficient integration. The Configuration Buffer stores decoding information such as the total number of layers, the current layer ID, request ID, and the token index (T_{cur}). The Va2Pa table and the Command Buffer are initialized with the virtual-to-physical address mapping of the KV-cache and the DPA-encoded PIM command stack, respectively. The host updates the Configuration Buffer each iteration with current decoding information, such as T_{cur} . Upon completing a request, the allocated memory chunk is released by updating the Va2Pa table, while the new request ID and associated T_{cur} are received. The Decoding Unit uses the Configuration Buffer, Command Buffer, and Va2Pa table to dispatch the corresponding PIM command sequence.

5.4 Use Case: Lazy Memory Allocation

Integrating the proposed DPA and on-module dispatcher enables lazy memory allocation, which dynamically adjusts PIM memory capacity based on requests' context lengths. The KV-cache increases with each iteration and eventually exceeds the pre-allocated chunk capacity. At this point, the Va2Pa table is updated to allocate a new chunk to accommodate the additional KV-cache. As shown in Fig. 6(d), when Request-1 requires more capacity, the host allocates a new chunk and updates the Va2Pa table. Notably, the new chunk does not need to be adjacent to the previous one, allowing on-demand allocation in non-contiguous memory regions and improving memory utilization.

Lazy memory allocation also increases the batch size for pipeline parallelization. The host determines the batch size for each iteration of pipeline processing. Under static memory allocation, requests must be assigned memory sufficient for the maximum context length, which limits the number of requests that can be processed simultaneously, even when current requests have smaller context lengths. In contrast, lazy memory allocation uses a smaller number of non-contiguous chunks to handle requests with small KV-cache sizes, significantly

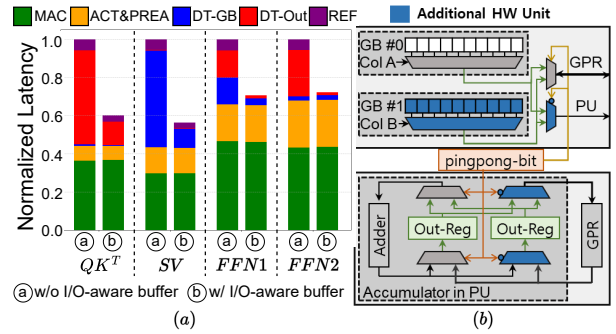


Figure 7: (a) Comparison of latency breakdowns for each LLM operation with and without I/O-aware buffering. (b) Illustration of the implementation details for I/O-aware buffering, including data flow and the ping-pong bit mechanism.

boosting average batch size. For example, the average batch size increases by up to 380% compared to static allocation, approaching near-optimal levels (Fig. 4). As discussed in Sec. 4, a larger effective batch size improves PIM's capacity utilization, reduces pipeline bubbles, and enhances throughput.

6 PIM I/O BOTTLENECK

I/O Bottleneck Analysis. While our mapping strategy improves LoL-PIM's efficiency for LLM inference, it doesn't address the I/O data transfer overhead inherent to it. LoL-PIM's buffers are significantly smaller than those in recent DRAM-PIM architectures [19, 54], limiting input and output data reuse. Fig. 7(a) reveals that data transfer latency for Out-Reg (DT-Out) and GB (DT-GB) accounts for over 50% of total latency in QK^T and SV operations. This highlights the need for architectural improvements in LoL-PIM to reduce input and output data transfer overhead.

I/O-aware buffering for Overcoming I/O Bottleneck. We propose *I/O-aware buffering*, strategy for LoL-PIM to address data transfer bottlenecks. It uses two buffer sets: one for current dot-product operations and another for preparing for the next, hiding transfer cycles within the computation. Fig. 7(b) illustrates *I/O-aware buffering* applied to input and output transfers via Global Buffer (GB) and Out-Reg. This approach maintains LoL-PIM's main computation datapath with minimal hardware changes: extended control logic (a pingpong-bit for alternating buffers), additional muxes for buffer selection, and an extra GB shared across banks. *I/O-aware buffering* leverages existing Out-Reg sets, suiting PIM's constrained environment.

Evaluation. To evaluate the proposed method, we modified LoL-PIM's control path in Ramulator [30], implementing a dual command queue and pingpong-bit mechanism. This allows intermittent execution blocking and bit reversal for subsequent commands. The MAC units' datapath remains unchanged, preserving critical path elements. The main overhead comes from the controller's pingpong-bit-based command execution and an extra GB. Area estimation using CACTI and Synopsys Design Compiler with SAED 32nm technology shows only a 1.7% increase for a 256-MAC unit. Fig. 7(a) demonstrates *I/O-aware buffering's* significant latency reductions: 40% in QK^T (overlapping DT-Out with DOT-PROD(MAC) latency), 44% in SV

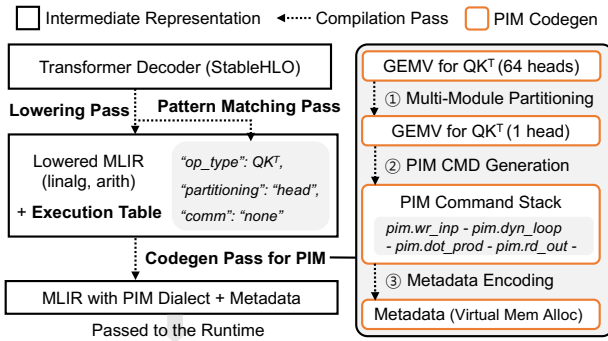


Figure 8: Overall compilation flow of LoL-PIM.

(overlapping DT-GB with DOT-PROD latency), 29% in FFN^1 and 28% in FFN^2 .

7 LOL-PIM SYSTEM ARCHITECTURE

We implement LoL-PIM as a software-hardware codesign to enable the proposed ideas of PIM-aware partitioning, dynamic memory management, and I/O aware buffering to enhance PIM’s capability for long-context LLM decoding. We extend the existing machine learning compiler framework to integrate PIM-specific compilation flow and code generation for diverse variants of Transformer decoding workloads. Also, we augment AiMX’s microarchitecture to enable on-module command dispatching and I/O aware buffering.

7.1 Multi-PIM Compiler and Runtime

We extend a popular compiler framework, MLIR [37], to enable seamless mapping of various LLM operations to the PIM command stack. MLIR’s multi-level abstractions, ranging from high-level tensor computations (e.g., *linalg.batch_matmul*) to hardware-centric operations (e.g., *pim.wr_inp*), facilitate customized optimizations and transformations for multi-PIM architectures. A runtime launches the compiled PIM command stacks on the multi-PIM environment. We extend IREE [62] and its hardware abstraction layer (HAL) to integrate PIM’s software development kit (SDK) for memory allocation and command dispatching in end-to-end LLM inference¹.

Compiling Transformer Variants. Fig. 8 illustrates LoL-PIM’s compilation workflow. The *Lowering Pass* starts with the processing of Transformer decoder operations represented in the *StableHLO* dialect [60] and translating them into lower-level MLIR dialects like *linalg* and *arith*. Mapping Transformer operations of varying sizes and structures is a key challenge. To address this, we implement a *Pattern-Matching Pass* that extends existing IR traversal to identify sequences of operation types matching predefined decoder patterns like GQA and SwiGLU. In the case of GQA, for example, we detect mismatched vector dimensions between Q and K, V . Upon pattern matching, the compiler generates *Execution Table* specifying the Transformer operation type, partitioning direction, and communication strategy for each operation.

¹We implement our LoL-PIM framework using MLIR and IREE Ver. Feb. 18, 2023. (commit eb14186) and (commit 2f40854), respectively. We integrate the AiMX vendor library (AiM-SDK) into our runtime and validate our PIM simulation setup by using AiM-SDK’s software simulator.

LoL-PIM	Composition	8 Modules, 16 AiM controllers per Module
	Frequency	1GHz
	Interface Bandwidth	64GB/s
HUB	GPR (SRAM)	512KB
	Compute Unit	Softmax, Layernorm, EWADD, EWMUL
	Dispatcher	DPA CMD buffer(96KB), Addr Map Buffer(96KB)
AiM	Memory Configuration	GDDR6 16Gb/s; x16 organization; 512 GB/s; 2 channels per chip; 16 channels; 16 banks/Channel; Page size = 2KB
	Processing Unit (PU)	1 PU per bank; 32 GFLOPS per PU(with 1 GHz)
	Global Buffer	2KB Global Buffer per channel

Table 5: LoL-PIM’s hardware configurations.

PIM Command Generation. We implemented *PIM Dialect* in the *Codegen Pass* to convert the lowered Transformer operations into the PIM command stack. *PIM Dialect* consists of two main steps: 1) PIM-aware multi-module partitioning and 2) microcoding for PIM command generation. For instance, given the number of PIM modules and workload information (LLM structure, context length, batch size), QK^T ’s GEMV workload is partitioned and distributed to multiple PIM modules (①). For each module, the loop-based PIM command generation step constructs a command stack for the partitioned QK^T computation. Since the same computation patterns repeat across Transformer decoder layers and tokens, a PIM command stack is encoded with DPA for compact representation(②). The necessary metadata for runtime dispatching, especially the virtual memory allocation for the weights and KV-cache are also encoded (③).

7.2 Hardware Overhead.

To construct the LoL-PIM hardware, a on-module dispatcher is introduced to the HUB to support dynamic memory management, and a I/O-aware buffer is applied to AiM to overcome the I/O bottleneck. To evaluate the overhead of these two hardware components, we use the PIM architecture from [70] as the baseline, with the AiM architecture based on information from [31]. The baseline PIM architecture consists of 2 HUBs and a total of 16 AiMs [70]. To model our LoL-PIM, the on-module dispatcher and I/O-aware buffer are applied to the HUB and AiM, respectively, in the baseline PIM. Since the most dominant hardware component in this PIM architecture is the AiM, the overhead of the I/O-aware buffer is modeled as a percentage of the hardware area of a single AiM chip, while the overhead of the on-module dispatcher is modeled as a percentage of the area corresponding to eight AiMs.

The area of a single AiM, which consists of 16 PUs and 16 bank cells, is approximately 12.16 mm² [31]. Firstly, for the overhead of the I/O-aware buffer, the 2KB area required for additional Global Buffer is modeled using CACTI, resulting in an area of 0.053 mm², which corresponds to an overhead of approximately 0.4%. Secondly, the on-module dispatcher requires a Va2Pa Table, CMD Buffer, configuration buffer, and a decoding unit. The area for the decoding unit is modeled using Synopsys Design Compiler under SAED 32nm technology, while the buffers are modeled using CACTI, resulting in a total area of 0.48 mm². Since one on-module dispatcher is required per eight AiMs, the total overhead for the entire PIM system is approximately 0.5%.

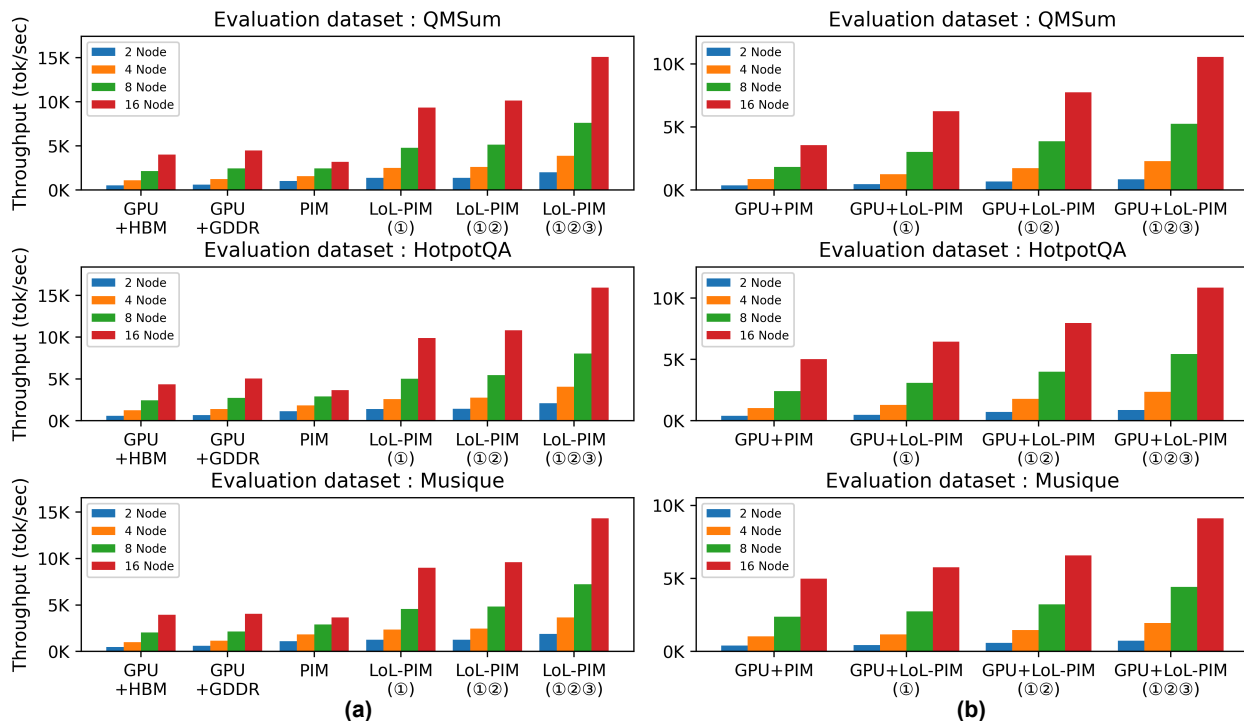


Figure 9: Throughput evaluation of Qwen1.5-7B on standalone (a) and heterogeneous (b) systems. The throughput (tokens/sec) is measured on QMSum HotpotQA and Musique tasks.

Matrix shape	(4096, 8192)	(4096, 16384)	(8192, 4096)	(12288, 12288)
Cycle Diff.	0.73%	0.79%	0.89%	0.78%

Table 6: Validation of our Ramulator-based PIM simulator (cycle difference with the AiMX vendor library).

8 EVALUATION

8.1 Evaluation Settings

Evaluation LLMs. We evaluate LoL-PIM’s compiler capability using diverse LLMs specified in Table 1, with 1.8B to 72B parameters, considering context lengths up to 32K tokens, and popular activation types (RELU, SwiGLU) implemented in AiM’s LUT. We also consider three tasks with distinct context length characteristics from a representative long-context LLM benchmarks, LongBench [8]; QM-Sum (Summarization), HotpotQA and Musique (Multi-Document QA) (Table 2).

Baselines. We evaluate our system against three baselines: (1) a 16-GPU DGX-A100 system, each GPU equipped with 80GB HBM3 and simulated using a DGX simulator (GPU-HBM), (2) 16 AiMX cards, each comprising 8 devices with one Xilinx Virtex UltraScale+VU9P FPGA and eight 1GB AiM chips utilizing GDDR6 and QSFP links for inter-card communication (PIM), and (3) a GPU-only system using GDDR6 for GPU evaluation with the matched external bandwidth of the PIM system (GPU-GDDR). These baselines were simulated using validated tools, including the DGX simulator [24] and our extended version of Ramulator [30], which we validated to

		GPU-HBM (A100[51])	GPU-GDDR6	PIM
Compute	Frequency	1.4GHz	1.4GHz	1.0GHz
	Peak FLOPS	312T	312T	66T
Off-chip	Type	HBM3	GDDR6	GDDR6
	Capacity	80GB	64GB	64GB
Memory	External BW	3352GB/s	4096GB/s	4096GB/s
	Internal BW	N/A	N/A	65.5TB/s

Table 7: Specification of GPU-HBM, GPU-GDDR, and PIM(=LoL-PIM).

ensure accuracy (see Table 6). This setup enables a comprehensive comparison of LLM inference performance across architectures. Detailed specifications for the baselines are provided in Table 7.

LoL-PIM. We model LoL-PIM’s latency using a modified Ramulator implementation, validated against AiM-SDK and based on reference design parameters (Table 6). The simulation includes AiM’s core functionality, AiMX’s multicasting interconnect, and power models derived from DRAM references and CACTI. To evaluate performance comprehensively, we test LoL-PIM with three key techniques: ① scalable PIM architecture, ② dynamic PIM memory management, and ③ I/O-aware buffering. Inspired by recent advances in heterogeneous PIM systems [19, 54, 57], we examine LoL-PIM in both standalone and hybrid GPU+PIM configurations (the hybrid configuration halving PIM capacity). All systems, including the baselines and LoL-PIM (①,②,③), are configured to have a matched

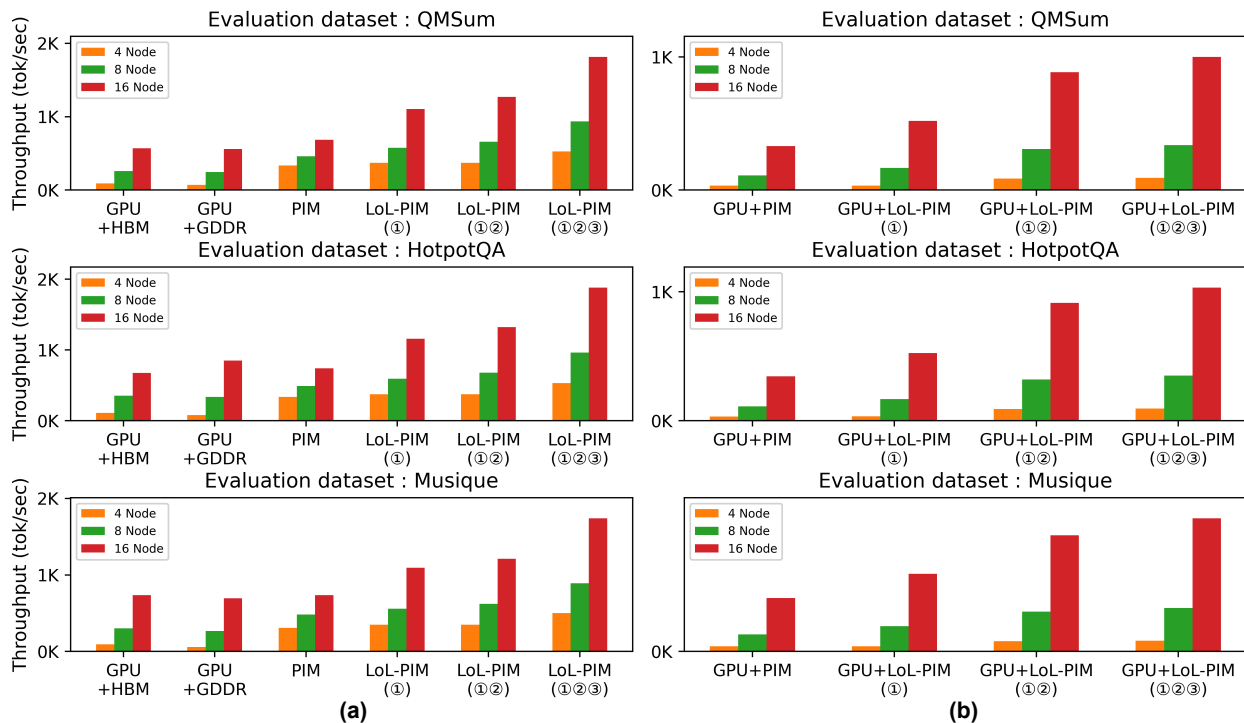


Figure 10: Throughput evaluation of Qwen1.5-72B on standalone (a) and heterogeneous (b) systems. The throughput (tokens/sec) is measured on QMSum HotpotQA and Musique tasks.

external memory bandwidth². Multi-node communication latency is modeled conservatively at 10GB/s, aligned with AiMX card QSFP bandwidth and matched across systems. Table 5 outlines LoL-PIM’s architectural parameters.

8.2 Performance Comparison

Scalability. We evaluate LoL-PIM’s scalability across three long-context LLM benchmarks (Table 2), focusing on the Qwen1.5-7B model (Fig. 9(a)). The baseline PIM-only system showed the poorest scalability due to inefficient PIM utilization. While it outperformed the GPU-only system at a smaller capacity of 128GB, its scalability limitations led to the lowest performance at the largest capacity of 1024GB, highlighting the drawbacks of conventional PIM mapping approaches at larger scales. In contrast, LoL-PIM demonstrated significantly better scalability. At 1024GB, it outperformed the baseline GPU-GDDR and PIM-only systems by 3.54× and 4.74×, respectively, showcasing its superior efficiency. This improvement stems from two key factors: (1) pipeline parallelization, which sustains tensor parallelization and prevents PIM channel utilization drops at larger scales, and (2) larger batch sizes enabled by scaling, which reduce pipeline bubble overhead and enhance throughput³. A similar trend was observed with the Qwen1.5-72B model (Fig. 9(b)). The baseline PIM-only system again exhibited the lowest scalability

and was unable to execute the 72B model on a 128GB system due to its parameter size. However, for capacities between 256GB and 1024GB, LoL-PIM consistently outperformed both the baseline GPU-GDDR and PIM-only systems by 8.54× and 2.65×, respectively. These results underscore LoL-PIM’s capability to efficiently handle larger models with substantial memory and computational demands. Its sustained high throughput across increasing system capacities highlights its robustness and effectiveness in scaling large-scale workloads.

Standalone vs. Heterogeneous Systems. We further compare the scalability of standalone and the heterogeneous systems. Prior works [19, 54, 57] have suggested promising performance of the heterogeneous xPU+PIM architectures, yet they have not been carefully evaluated in the long-context LLM workloads. In Fig. 9 and Fig. 10, we compare the throughput of the standalone and heterogeneous systems for 7B and 72B models, respectively. Each system was evaluated with capacities ranging from 128GB to 1024GB, showcasing the average tokens per second (tok/sec) achieved while processing the evaluation dataset. Although showing scalability in general, GPU+LoL-PIM achieves inferior throughputs compared to the standalone systems (LoL-PIM). This disatisfactory performance is due to the long-context LLM’s memory-bounded characteristics; the higher throughput can be achieved with the more internal memory bandwidth. Yet, the speedup of PIM-only system over GPU+PIM is less than the internal memory bandwidth gap (2×) thanks to

²The system does not compromise inference accuracy.

³GPU-GDDR is evaluated to match the external bandwidth with PIM-only systems

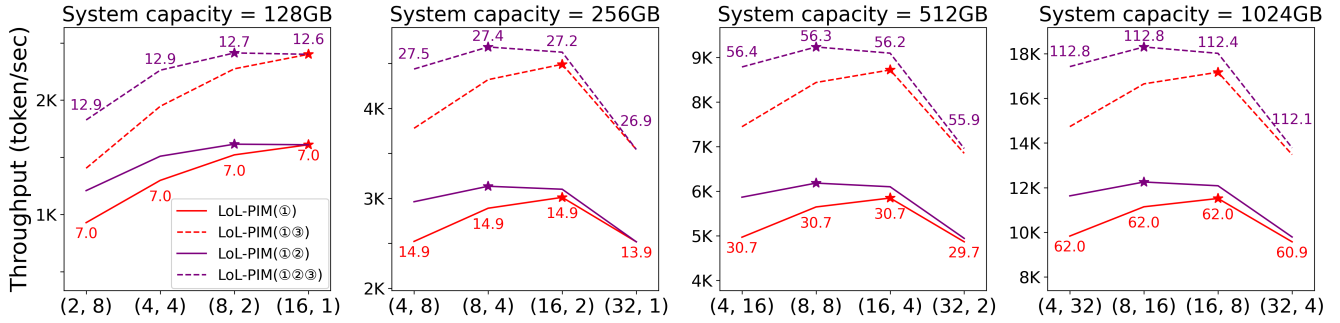


Figure 11: Throughput (tokens/sec) measured on Musique with Qwen-7B. The x-axis indicates the combinations of Tensor Parallel (TP) and Pipeline Parallel (PP) across all nodes. The numbers above each point represent the average batch size.

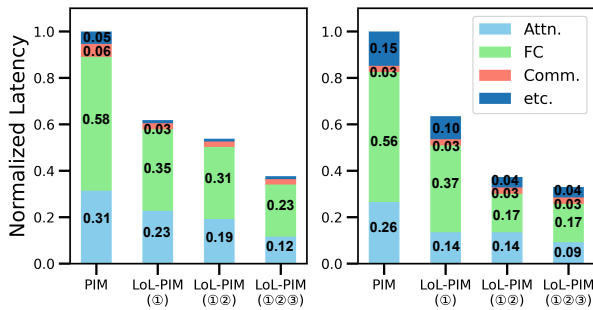


Figure 12: Latency breakdown of LLM operations on Qwen1.5-72B for LoL-PIM, comparing two configurations. The left plot represents the result in a standalone and the right plot represents the result in a heterogeneous configuration.

GPU+PIM’s efficiency in avoiding underutilization for FC layers. Still, the proposed scalable PIM partitioning, dynamic PIM memory management, and I/O-aware buffering consistently improve the GPU+PIM’s performance, similar to the PIM-only systems.

8.3 Ablation Study

Tensor vs. Pipeline Parallelization. LoL-PIM (⊕) employs a token-parallel approach to maximize pipeline parallelism. However, increasing the number of pipeline stages introduces pipeline bubbles, which reduce utilization. These overheads diminish with larger batch sizes, necessitating different pipeline parallelism strategies depending on the presence of dynamic PIM memory management. Fig. 11 shows how the optimal balance of tensor and pipeline parallelism varies with and without DPA across system scales. With fixed parallelism strategies, DPA improves performance by up to 1.3×. Additionally, under the same DPA condition, performance differences between parallelism combinations can reach 1.73×. The performance gap between optimal parallelism points with and without dynamic memory management is up to 7%, underscoring the sensitivity of LoL-PIM (⊕) to dynamic adjustments in batch size and parallelism strategies.

Latency Breakdown. Fig. 12 highlights LoL-PIM’s effectiveness compared to baseline GPU and PIM systems. For the 72B model, the large weight parameters and KV cache sizes lead to smaller

Model	#PIM	PIM		LoL-PIM (⊕⊙)		LoL-PIM (⊕⊙⊕)	
Scale	Node	Token/sec	Util.	Token/sec	Util.	Token/sec	Util.
7B	4	1833	15.1	2455	20.2	3668	30.1
14B	5	1309	15.4	1737	20.5	2553	30.1
72B	16	737	12.8	1211	21.1	1740	30.3

Table 8: Throughput (token/sec) and utilization (%) for various LLM scales (Qwen series), measured on Musique.

Model	Context	QMSum	HotpotQA	Musique	Avg.
Mistral-7B	32K	25.55	49.77	28.20	34.51
	16K	25.36	49.97	27.67	34.33
	8K	24.13	43.63	23.49	30.42
	4K	21.51	40.30	19.84	27.22
Qwen1.5-7B	32K	23.92	48.11	26.74	32.92
	16K	23.32	46.78	28.24	32.78
	8K	21.65	44.29	27.64	31.19
	4K	20.61	38.05	19.02	25.89

Table 9: Accuracy evaluation of three LongBench tasks with limited context length for Mistral-7B and Qwen1.5-7B.

batch sizes, causing memory-bound issues in FC operations. This is particularly evident in hybrid systems, where GPU batch processing provides limited acceleration, resulting in significant FC overhead. LoL-PIM’s token-parallel approach (⊕) addresses these inefficiencies by reducing memory overhead in the KV cache, minimizing both Attention and FC bottlenecks. Enhancements with (⊕⊙) further increase average batch size, with greater benefits observed in heterogeneous systems. Additional latency reduction is achieved through I/O-aware buffering (⊕⊙⊕). Overall, these combined improvements reduce latency by over 60% for both standalone and heterogeneous systems, demonstrating the effectiveness of the proposed methods.

Utilization Trends in Scaling LLM Size. To demonstrate LoL-PIM’s scalability for LLM inference workloads, we focus on utilization trends across models scaling from 7B to 72B parameters compare with baseline PIM-only systems. The node count is proportionally increased to ensure sufficient memory for larger models. The baseline PIM system exhibits consistently low utilization rates, with a pronounced decline as model scale increases, particularly for the 72B model, where utilization drops to 12.8%. In contrast, LoL-PIM (⊕⊙⊕) shows a significant improvement, nearly doubling the utilization of the baseline PIM system and maintaining a stable utilization rate of around 30%, even for larger models. This sustained

utilization across different model sizes (as summarized in Table 8) demonstrates the critical role of ITTPP, DPA and I/O-aware buffering in achieving scalable LLM inference.

Impact of Context Length on Accuracy in LLM Inference. To justify developing an efficient long-context LLM serving system, we evaluated two popular long-context LLMs from Table 1 on three LongBench tasks: QMSum, HotpotQA, and Musique (context characteristics in Table 2). We used fixed max context lengths ranging from 4K to 32K, truncating exceeding contexts as per LongBench guidelines [8]. Table 9 shows that context truncation from 4K to 32K significantly degrades LLM inference accuracy by 13.8-29.6%. While shorter contexts enable faster token generation (Fig.3), this speed-up may not justify the accuracy loss in performance-sensitive tasks requiring precise information retrieval from user contexts. This underscores the value of LoL-PIM, a scalable multi-node LLM serving system based on resource-effective, domain-specific PIMs.

9 RELATED WORK

Multi-Node LLM Serving. As LLMs scale, they require more memory and bandwidth, making parallelization techniques like tensor [59] and pipeline parallelization [50] essential for LLM serving. Advanced serving systems [1, 2, 9] now incorporate continuous batching [71] and efficient KV cache management [33] to improve GPU utilization. However, recent studies reveal GPU underutilization in multi-GPU LLM serving, especially during token generation, leading to approaches leveraging hardware heterogeneity [17, 55]. This paper proposes a multi-node, PIM-only LLM serving system to address GPU underutilization and presents an efficient parallelization strategy for multi-node environments.

DRAM-Based PIM. DRAM-based Processing-in-Memory (PIM) has become a key commercial solution for accelerating computational tasks, especially for Large Language Models (LLMs). This includes general-purpose solutions like UPMEM-PIM [16, 23, 47] and domain-specific accelerators such as HBM-PIM [27–29, 36, 39] and AiM [18, 32, 41], optimized for matrix multiplication. Recent research addresses bottlenecks in homogeneous PIM environments [26, 74] and heterogeneous xPU-PIM configurations [19, 42, 54, 57, 65]. The introduction of AiMX [34, 35], combining FPGA with AiM chips, marks a significant advancement in computational support and parallel processing for LLMs, reflecting the industry’s move towards more efficient, specialized hardware.

10 CONCLUSIONS

We introduce LoL-PIM, a multi-node PIM acceleration system addressing these issues. It features advanced parallelism techniques, direct PIM access commands and on-module dispatcher, and I/O-aware buffering for reducing I/O transfer overhead. Evaluations show LoL-PIM significantly enhances throughput and reduces latency for long-context LLM inference, outperforming multi-GPU and GPU-PIM systems (up to 8.54× and 16.0× speedup, respectively), enabling more efficient LLM deployment.

REFERENCES

[1] 2023. *DeepSpeed-FastGen*. <https://github.com/NVIDIA/TensorRT-LLM> Accessed on: 2024-04-01.

[2] 2023. *NVIDIA TensorRT-LLM*. <https://github.com/NVIDIA/TensorRT-LLM> Accessed on: 2024-04-01.

[3] Amey Agrawal, Nitin Kedia, Ashish Panwar, Jayashree Mohan, Nipun Kwatra, Bhargav Gulavani, Alexey Tumanov, and Ramachandran Ramjee. 2024. Taming Throughput-Latency Tradeoff in LLM Inference with Sarathi-Serve. In *18th USENIX Symposium on Operating Systems Design and Implementation (OSDI 24)*. USENIX Association, Santa Clara, CA, 117–134. <https://www.usenix.org/conference/osdi24/presentation/agrawal>

[4] Joshua Ainslie, James Lee-Thorp, Michiel de Jong, Yury Zemlyanskiy, Federico Lebrón, and Sumit Sanghai. 2023. GQA: Training Generalized Multi-Query Transformer Models from Multi-Head Checkpoints. arXiv:2305.13245 [cs.CL] <https://arxiv.org/abs/2305.13245>

[5] Reza Yazdani Aminabadi, Samyam Rajbhandari, Minjia Zhang, Ammar Ahmad Awan, Cheng Li, Du Li, Elton Zheng, Jeff Rasley, Shaden Smith, Olatunji Ruwase, and Yuxiong He. 2022. DeepSpeed Inference: Enabling Efficient Inference of Transformer Models at Unprecedented Scale. arXiv:2207.00032 [cs.LG] <https://arxiv.org/abs/2207.00032>

[6] Kazi Asifuzzaman, Narasinga Rao Miniskar, Aaron R. Young, Frank Liu, and Jeffrey S. Vetter. 2023. A survey on processing-in-memory techniques: Advances and challenges. *Memories - Materials, Devices, Circuits and Systems* 4 (2023), 100022. <https://doi.org/10.1016/j.memori.2022.100022>

[7] Jinze Bai, Shuai Bai, Yunfei Chu, Zeyu Cui, Kai Dang, Xiaodong Deng, Yang Fan, Wenbin Ge, Yu Han, Fei Huang, Binyuan Hui, Luo Ji, Mei Li, Junyang Lin, Runji Lin, Dayiheng Liu, Gao Liu, Chengqiang Lu, Keming Lu, Jianxin Ma, Rui Men, Xingzhang Ren, Xuancheng Ren, Chuanqi Tan, Sinan Tan, Jianhong Tu, Peng Wang, Shijie Wang, Wei Wang, Shengguang Wu, Benfeng Xu, Jin Xu, An Yang, Hao Yang, Jian Yang, Shusheng Yang, Yang Yao, Bowen Yu, Hongyi Yuan, Zheng Yuan, Jianwei Zhang, Xingxuan Zhang, Yichang Zhang, Zhenru Zhang, Chang Zhou, Jingren Zhou, Xiaohuan Zhou, and Tianhang Zhu. 2023. Qwen Technical Report. arXiv:2309.16609 [cs.CL] <https://arxiv.org/abs/2309.16609>

[8] Yushi Bai, Xin Lv, Jiajie Zhang, Hongchang Lyu, Jiankai Tang, Zhidian Huang, Zhengxiao Du, Xiao Liu, Aohan Zeng, Lei Hou, Yuxiao Dong, Jie Tang, and Juanzi Li. 2024. LongBench: A Bilingual, Multitask Benchmark for Long Context Understanding. arXiv:2308.14508 [cs.CL] <https://arxiv.org/abs/2308.14508>

[9] Jaehong Cho, Minsu Kim, Hyunmin Choi, and Jongse Park. 2024. LLM-Sim: A Simulation Infrastructure for LLM Inference Serving Systems. In *Machine Learning for Computer Architecture and Systems 2024*. <https://openreview.net/forum?id=LJ2IUf18km>

[10] Jaewan Choi, Jaehyun Park, Kwanhee Kyung, Nam Sung Kim, and Jung Ho Ahn. 2023. Unleashing the Potential of PIM: Accelerating Large Batched Inference of Transformer-Based Generative Models. *IEEE Computer Architecture Letters* (2023).

[11] Claude. 2024. Claude 3.5 Sonnet. <https://www.anthropic.com/news/claude-3-5-sonnet>. Accessed on: 2024-11-21.

[12] Tri Dao, Daniel Haziza, Francisco Massa, and Grigory Sizov. 2023. Flash-decoding for long-context inference. Online. <https://crfm.stanford.edu/2023/10/12/flashdecoding.html>.

[13] Peter Druschel, Antoine Kaufmann, Jonathan Mace, Jason Flinn, Margo Seltzer, Woosuk Kwon, Zhuohan Li, Siyuan Zhuang, Ying Sheng, Lianmin Zheng, Cody Hao Yu, Joseph Gonzalez, Hao Zhang, and Ion Stoica. 2023. Efficient Memory Management for Large Language Model Serving with PagedAttention. *Proceedings of the 29th Symposium on Operating Systems Principles* (2023), 611–626. <https://doi.org/10.1145/3600006.3613165> arXiv:2309.06180

[14] Abhimanyu Dubey, Abhinav Jauhri, Abhinav Pandey, Abhishek Kadian, Ahmad Al-Dahle, Aiesha Letman, Akhil Mathur, Alan Schelten, Amy Yang, Angela Fan, Anirudh Goyal, Anthony Hartshorn, Aobo Yang, Archi Mitra, Archie Sravankumar, Artem Korenev, Arthur Hinsvark, Arun Rao, Aston Zhang, Aurelien Rodriguez, Austen Gregerson, Ava Spataru, Baptiste Roziere, Bethany Biron, Binh Tang, Bobbie Chern, Charlotte Caucheteux, Chaya Nayak, Chloe Bi, Chris Marra, Chris McConnell, Christian Keller, Christophe Touret, Chunyang Wu, Corinne Wong, Cristian Canton Ferrer, Cyrus Nikolaidis, Damien Allonsius, Daniel Song, Danielle Pintz, Danny Livshits, David Esiobu, Dhruv Choudhary, Dhruv Mahajan, Diego Garcia-Olano, Diego Perino, Dieuwke Hupkes, Egor Lakomkin, Ehab AlBadawy, Elina Lobanova, Emily Dinan, Eric Michael Smith, Filip Radenovic, Frank Zhang, Gabriel Synnaeve, Gabrielle Lee, Georgia Lewis Anderson, Graeme Nail, Gregoire Mialon, Guan Pang, Guillem Cucurell, Hailey Nguyen, Hannah Korevaar, Hu Xu, Hugo Touvron, Iliyan Zarov, Imanol Arrieta Ibarra, Isabel Kloumann, Ishan Misra, Ivan Evtimov, Jade Copet, Jaewon Lee, Jan Geffert, Jana Vranes, Jason Park, Jay Mahadeokar, Jeet Shah, Jelmer van der Linde, Jennifer Billock, Jenny Hong, Jenya Lee, Jeremy Fu, Jianfeng Chi, Jianyu Huang, Jiawen Liu, Jie Wang, Jiecao Yu, Joanna Bitton, Joe Spisak, Jongsoo Park, Joseph Rocca, Joshua Johnstun, Joshua Saxe, Junteng Jia, Kalyan Vasuden Alwala, Kartikeya Upasani, Kate Plawiak, Ke Li, Kenneth Heafield, Kevin Stone, Khalid El-Arini, Krithika Iyer, Kshitiz Malik, Kuenley Chiu, Kunal Bhalala, Lauren Rantala-Yeara, Laurens van der Maaten, Lawrence Chen, Liang Tan, Liz Jenkins, Louis Martin, Lovish Madaan, Lubo Malo, Lukas Blecher, Lukas Landzaat, Luke de Oliveira, Madeline Muzzi, Mahesh Pasupuleti, Mannat Singh, Manohar Paluri, Marcin Kardas, Mathew Oldham, Mathieu Rita, Maya Pavlova, Melanie Kambadur, Mike Lewis, Min Si, Mitesh Kumar Singh, Mona Hassan, Naman Goyal, Narjes Torabi, Nikolay Bashlykov, Nikolay Bogoychev, Niladri Chatterji, Olivier Duchenne, Onur

- Celebi, Patrick Alrassy, Pengchuan Zhang, Pengwei Li, Petar Vasic, Peter Weng, Prajjwal Bhargava, Pratik Dubal, Praveen Krishnan, Punit Singh Koura, Puxin Xu, Qing He, Qingxiao Dong, Raghavan Srinivasan, Raj Ganapathy, Ramon Calderer, Ricardo Silveira Cabral, Robert Stojnic, Roberta Raileanu, Rohit Girdhar, Rohit Patel, Romain Sauvestre, Ronnie Polidoro, Roshan Sumbaly, Ross Taylor, Ruan Silva, Rui Hou, Rui Wang, Saghar Hosseini, Sahana Chennabasappa, Sanjay Singh, Sean Bell, Seohyun Sonia Kim, Sergey Edunov, Shao-liang Nie, Sharan Narang, Sharrath Rapparth, Sheng Shen, Shengye Wan, Shruti Bhosale, Shun Zhang, Simon Vandenhende, Soumya Batra, Spencer Whitman, Sten Sootla, Stephane Collet, Suchin Gururangan, Sydney Borodinsky, Tamar Herman, Tara Fowler, Tarek Sheasha, Thomas Georgiou, Thomas Scialom, Tobias Speckbacher, Todor Mihaylov, Tong Xiao, Ujjwal Karn, Vedanuj Goswami, Vibhor Gupta, Vignesh Ramanathan, Viktor Kerkez, Vincent Gonguet, Virginie Do, Vish Vogeti, Vladan Petrovic, Weiwei Chu, Wenhan Xiong, Wenyin Fu, Whitney Meers, Xavier Martinet, Xiaodong Wang, Xiaoqing Ellen Tan, Xinfeng Xie, Xuchao Jia, Xuewei Wang, Yaelle Goldschlag, Yashesh Gaur, Yasmine Babaei, Yi Wen, Yiwen Song, Yuchen Zhang, Yue Li, Yuning Mao, Zacharie Delpeyre Couderc, Zheng Yan, Zhengxing Chen, Zoe Papakipos, Aaditya Singh, Aaron Grattafiori, Abha Jain, Adam Kelsey, Adam Shajnfeld, Adithya Gangidi, Adolfo Victoria, Ahuva Goldstand, Ajay Menon, Ajay Sharma, Alex Boesenberg, Alex Vaughan, Alexei Baevski, Allie Feinstein, Amanda Kallet, Amit Sangani, Anam Yunus, Andrei Lupu, Andres Alvarado, Andrew Caples, Andrew Gu, Andrew Ho, Andrew Poulton, Andrew Ryan, Ankit Ramchandani, Annie Franco, Aparajita Saraf, Arkabandhu Chowdhury, Ashley Gabriel, Ashwin Barambe, Assaf Eisenman, Azadeh Yazdan, Beau James, Ben Maurer, Benjamin Leonhardi, Bernie Huang, Beth Loyd, Beto De Paola, Bhargavi Paranjape, Bing Liu, Bo Wu, Boyu Ni, Braden Hancock, Bram Wasti, Brandon Spence, Brani Stojkovic, Brian Gamido, Britt Montalvo, Carl Parker, Carly Burton, Catalina Mejia, Changhan Wang, Changkyu Kim, Chao Zhou, Chester Hu, Ching-Hsiang Chu, Chris Cai, Chris Tindal, Christoph Feichtenhofer, Damon Civin, Dana Beaty, Daniel Kreymer, Daniel Li, Danny Wyatt, David Adkins, David Xu, Davide Testuggine, Delia David, Devi Parikh, Diana Liskovich, Didem Foss, Dingkang Wang, Duc Le, Dustin Holland, Edward Dowling, Eissa Jamil, Elaine Montgomery, Eleonora Presani, Emily Hahn, Emily Wood, Erik Brinkman, Esteban Arcaute, Evan Dunbar, Evan Smothers, Fei Sun, Felix Kreuk, Feng Tian, Firat Ozgenel, Francesco Caggioni, Francisco Guzman, Frank Kanayet, Frank Seide, Gabriela Medina Florez, Gabriella Schwarz, Gada Badeer, Georgia Swee, Gil Halpern, Govind Thattai, Grant Herman, Grigory Sizov, Guangyi, Zhang, Guna Lakshminarayanan, Hamid Shojanazeri, Han Zou, Hannah Wang, Hanwen Zha, Haroun Habeeb, Harrison Rudolph, Helen Suk, Henry Aspegren, Hunter Goldman, Ibrahim Damlaj, Igor Molybog, Igor Tufanov, Irina-Elena Veliche, Itai Gat, Jake Weissman, James Geboski, James Kohli, Japhet Asher, Jean-Baptiste Gaya, Jeff Marcus, Jeff Tang, Jennifer Chan, Jenny Zhen, Jeremy Reizenstein, Jeremy Teboul, Jessica Zhong, Jian Jin, Jingyi Yang, Joe Cummings, Jon Carvill, Jon Shepard, Jonathan McPhee, Jonathan Torres, Josh Ginsburg, Junjie Wang, Kai Wu, Kam Hou U, Karan Saxena, Kartik Prasad, Kartikay Khandelwal, Katayoun Zand, Kathy Matosich, Kaushik Veeraraghavan, Kelly Michelena, Keqian Li, Kun Huang, Kunal Chawla, Kushal Lakhotia, Kyle Huang, Lailin Chen, Lakshya Garg, Lavender A, Leandro Silva, Lee Bell, Lei Zhang, Liangpeng Guo, Licheng Yu, Liron Moshkovich, Luca Wehrstedt, Madian Khabza, Manav Avalani, Manish Bhatt, Maria Tsimpoukelli, Martynas Mankus, Matan Hasson, Matthew Lennie, Matthias Reso, Maxim Groshev, Maxim Naumov, Maya Lathi, Meghan Keneally, Michael L. Seltzer, Michal Valko, Michelle Restrepo, Mihir Patel, Mik Vyatskov, Mikayel Samvelyan, Mike Clark, Mike Macey, Mike Wang, Miquel Jubert Hermoso, Mo Metanat, Mohammad Rastegari, Munish Bansal, Nandhini Santhanam, Natascha Parks, Natasha White, Navyata Bawa, Nayan Singhal, Nick Egebo, Nicolas Usunier, Nikolay Pavlovich Laptev, Ning Dong, Ning Zhang, Norman Cheng, Oleg Chernoguz, Olivia Hart, Omkar Salpekar, Ozlem Kalinli, Parkin Kent, Parth Parekh, Paul Saab, Pavan Balaji, Pedro Rittner, Philip Bontrager, Pierre Roux, Piotr Dollar, Polina Zvyagina, Prashant Ratanchandani, Pritish Yuvraj, Qian Liang, Rachad Alao, Rachel Rodriguez, Rafi Ayub, Raghotham Murthy, Raghu Nayani, Rahul Mitra, Raymond Li, Rebekkah Hogan, Robin Battey, Rocky Wang, Rohan Maheswari, Russ Howes, Rutu Rinott, Sai Jayesh Bondu, Samyak Datta, Sara Chugh, Sara Hunt, Sargun Dhillon, Sasha Sidorov, Satadru Pan, Saurabh Verma, Seiji Yamamoto, Sharadh Ramaswamy, Shaun Lindsay, Shaun Lindsay, Sheng Feng, Shenghao Lin, Shengxin Cindy Zha, Shiva Shankar, Shuqiang Zhang, Shuqiang Zhang, Sinong Wang, Sneha Agarwal, Soji Sajuyigbe, Soumith Chintala, Stephanie Max, Stephen Chen, Steve Kehoe, Steve Satterfield, Sudarshan Govindaprasad, Sumit Gupta, Sungmin Cho, Sunny Virk, Suraj Subramanian, Sy Choudhury, Sydney Goldman, Tal Remez, Tamar Glaser, Tamara Best, Thilo Kohler, Thomas Robinson, Tianhe Li, Tianjun Zhang, Tim Matthews, Timothy Chou, Tzook Shaked, Varun Vontimitta, Victoria Ajayi, Victoria Montanez, Vijai Mohan, Vinay Satish Kumar, Vishal Mangla, Vitor Albiero, Vlad Ionescu, Vlad Poenaru, Vlad Tiberiu Mihalescu, Vladimir Ivanov, Wei Li, Wenchen Wang, Wenwen Jiang, Wes Bouaziz, Will Constable, Xiaocheng Tang, Xiaofang Wang, Xiaoqian Wu, Xiaolan Wang, Xide Xia, Xilun Wu, Xinbo Gao, Yanjun Chen, Ye Hu, Ye Jia, Ye Qi, Yenda Li, Yilin Zhang, Ying Zhang, Yossi Adi, Youngjin Nam, Yu, Wang, Yuchen Hao, Yundi Qian, Yuzi He, Zach Rait, Zachary DeVito, Zef Rosnbrick, Zhaoduo Wen, Zhenyu Yang, and Zhiwei Zhao. 2024. The Llama 3 Herd of Models. arXiv:2407.21783 [cs.AI] <https://arxiv.org/abs/2407.21783>
- [15] Alicia Golden, Samuel Hsia, Fei Sun, Bilge Acun, Basil Hosmer, Yejin Lee, Zachary DeVito, Jeff Johnson, Gu-Yeon Wei, David Brooks, et al. 2024. Is Flash Attention Stable? *arXiv preprint arXiv:2405.02803* (2024).
 - [16] Juan Gómez-Luna, Izzat El Hajj, Ivan Fernandez, Christina Giannoula, Geraldo F. Oliveira, and Onur Mutlu. 2022. Benchmarking a New Paradigm: Experimental Analysis and Characterization of a Real Processing-in-Memory System. *IEEE Access* 10 (2022), 52565–52608. <https://doi.org/10.1109/access.2022.3174101>
 - [17] Jiaao He and Jidong Zhai. 2024. FastDecode: High-Throughput GPU-Efficient LLM Serving using Heterogeneous Pipelines. arXiv:2403.11421 [cs.DC] <https://arxiv.org/abs/2403.11421>
 - [18] Mingxuan He, Choungki Song, Ilkon Kim, Chunseok Jeong, Seho Kim, Il Park, Mithuna Thottethodi, and TN Vijaykumar. 2020. Newton: A DRAM-maker’s accelerator-in-memory (AiM) architecture for machine learning. In *2020 53rd Annual IEEE/ACM International Symposium on Microarchitecture (MICRO)*. IEEE, 372–385.
 - [19] Guseul Heo, Sangyeop Lee, Jaehong Cho, Hyunmin Choi, Sanghyeon Lee, Hyungkyu Ham, Gwangsun Kim, Divya Mahajan, and Jongse Park. 2024. NeupIMs: A NPU-PIM Heterogeneous Acceleration for Batched Inference of Large Language Model. In *Proceedings of the 29th ACM International Conference on Architectural Support for Programming Languages and Operating Systems*. 1–16.
 - [20] Ke Hong, Guohao Dai, Jiaming Xu, Qiuli Mao, Xiuhong Li, Jun Liu, Kangdi Chen, Yuhuan Dong, and Yu Wang. 2023. Flashdecoding++: Faster large language model inference on gpus. *arXiv preprint arXiv:2311.01282* (2023).
 - [21] Seongmin Hong, Seungjae Moon, Junsoo Kim, Sungjae Lee, Minsub Kim, Dongsoo Lee, and Joo-Young Kim. 2023. DFX: A Low-Latency Multi-FPGA Appliance for Accelerating Transformer-Based Text Generation. In *Proceedings of the 55th Annual IEEE/ACM International Symposium on Microarchitecture (Chicago, Illinois, USA) (MICRO ’22)*. IEEE Press, 616–630. <https://doi.org/10.1109/MICRO56248.2022.00051>
 - [22] Yanping Huang, Youlong Cheng, Ankur Bapna, Orhan Firat, Mia Xu Chen, Dehao Chen, HyoukJoong Lee, Jiquan Ngiam, Quoc V Le, Yonghui Wu, et al. 2019. GPipe: Easy scaling with micro-batch pipeline parallelism. *proceeding of Computer Science > Computer Vision and Pattern Recognition* (2019).
 - [23] Bongjoon Hyun, Taehun Kim, Dongjae Lee, and Minsoo Rhu. 2023. Pathfinding Future PIM Architectures by Demystifying a Commercial PIM Technology. *arXiv* (2023). <https://doi.org/10.48550/arxiv.2308.00846> arXiv:2308.00846
 - [24] Jaehyun Park Jaewon Choi. 2024. Simulator for AttAcc. https://github.com/scale-snu/attach_simulator.
 - [25] Albert Q. Jiang, Alexandre Sablayrolles, Arthur Mensch, Chris Bamford, Devendra Singh Chaplot, Diego de las Casas, Florian Bressand, Gianna Lengyel, Guillaume Lample, Lucile Saulnier, Léo Renard Lavaud, Marie-Anne Lachaux, Pierre Stock, Teven Le Scao, Thibaut Lavril, Thomas Wang, Timothée Lacroix, and William El Sayed. 2023. Mistral 7B. arXiv:2310.06825 [cs.CL] <https://arxiv.org/abs/2310.06825>
 - [26] Hongju Kal, Chanyoung Yoo, and Won Woo Ro. 2023. AESPA: Asynchronous Execution Scheme to Exploit Bank-Level Parallelism of Processing-in-Memory. In *Proceedings of the 56th Annual IEEE/ACM International Symposium on Microarchitecture*. 815–827.
 - [27] Byeongho Kim, Sanghoon Cha, Sangsoo Park, Jieun Lee, Sukhan Lee, Shin-haeng Kang, Jinin So, Kyungsoo Kim, Jin Jung, Jong-Geon Lee, Sunjung Lee, Yoonah Paik, Hyeonsu Kim, Jin-Seong Kim, Won-Jo Lee, Yuhwan Ro, YeonGon Cho, Jin Hyun Kim, JoonHo Song, Jaehoon Yu, Seungwon Lee, Jeonghyeon Cho, and Kyomin Sohn. 2024. The Breakthrough Memory Solutions for Improved Performance on LLM Inference. *IEEE Micro* 44, 3 (2024), 40–48. <https://doi.org/10.1109/MM.2024.3375352>
 - [28] Jin Hyun Kim, Shin-Haeng Kang, Sukhan Lee, Hyeonsu Kim, Yuhwan Ro, Seungwon Lee, David Wang, Jihyun Choi, Jinin So, YeonGon Cho, et al. 2022. Aquabolt-XL HBM2-PIM, LPDDR5-PIM with in-memory processing, and AXDIMM with acceleration buffer. *IEEE Micro* 42, 3 (2022), 20–30.
 - [29] Jin Hyun Kim, Yuhwan Ro, Jinin So, Sukhan Lee, Shin-haeng Kang, YeonGon Cho, Hyeonsu Kim, Byeongho Kim, Kyungsoo Kim, Sangsoo Park, et al. 2023. Samsung PIM/PNM for Transfmer Based AI: Energy Efficiency on PIM/PNM Cluster. In *2023 IEEE Hot Chips 35 Symposium (HCS)*. IEEE Computer Society, 1–31.
 - [30] Yoongu Kim, Weikun Yang, and Onur Mutlu. 2016. Ramulator: A Fast and Extensible DRAM Simulator. *IEEE Computer Architecture Letters* 15, 1 (2016), 45–49. <https://doi.org/10.1109/LCA.2015.2414456>
 - [31] Daehan Kwon, Seongju Lee, Kyuyoung Kim, Sanghoon Oh, Joonhong Park, Gi-Moon Hong, Dongyoon Ka, Kyudong Hwang, Jeongje Park, Kyeongpil Kang, Jungyeon Kim, Junyeol Jeon, Nahsung Kim, Yongkee Kwon, Vladimir Kornijuk, Woojae Shin, Jongsoo Won, Minkyu Lee, Hyunha Joo, Haerang Choi, Guhyun Kim, Byeongju An, Jaewook Lee, Dongguk Ko, Younggun Jun, Ilwoong Kim, Choungki Song, Ilkon Kim, Chanwook Park, Seho Kim, Chunseok Jeong, Euicheol Lim, Dongkyun Kim, Jieun Jang, Il Park, Junhyun Chun, and Joohwan Cho. 2023. A 1ynn 1.25V 8Gb 16Gb/s/Pin GDDR6-Based Accelerator-in-Memory Supporting 1TFLOPS MAC Operation and Various Activation Functions for Deep

- Learning Application. *IEEE Journal of Solid-State Circuits* 58, 1 (2023), 291–302. <https://doi.org/10.1109/JSSC.2022.3200718>
- [32] Daehan Kwon, Seongju Lee, Kyuyoung Kim, Sanghoon Oh, Joonhong Park, Gi-Moon Hong, Dongyoon Ka, Kyudong Hwang, Jeongje Park, Kyeongpil Kang, Jungyeon Kim, Junyeol Jeon, Nahsung Kim, Yongkee Kwon, Vladimir Kornijcuk, Woojae Shin, Jongsoon Won, Minkyu Lee, Hyunha Joo, Haerang Choi, Guhyun Kim, Byeongju An, Jaewook Lee, Donguc Ko, Younggun Jun, Ilwoong Kim, Choungki Song, Ilkon Kim, Chanwook Park, Seho Kim, Chunseok Jeong, Euicheol Lim, Dongkyun Kim, Jieun Jang, Il Park, Junhyun Chun, and Joohwan Cho. 2023. A 1.25V 8Gb 16Gb/s/Pin GDDR6-Based Accelerator-in-Memory Supporting ITFLOPS MAC Operation and Various Activation Functions for Deep Learning Application. *IEEE Journal of Solid-State Circuits* 58, 1 (2023), 291–302. <https://doi.org/10.1109/JSSC.2022.3200718>
- [33] Woosuk Kwon, Zhuohan Li, Siyuan Zhuang, Ying Sheng, Lianmin Zheng, Cody Hao Yu, Joseph Gonzalez, Hao Zhang, and Ion Stoica. 2023. Efficient memory management for large language model serving with pagedattention. In *Proceedings of the 29th Symposium on Operating Systems Principles*. 611–626.
- [34] Yongkee Kwon, Guhyun Kim, Nahsung Kim, Woojae Shin, Jongsoon Won, Hyunha Joo, Haerang Choi, Byeongju An, Gyeongcheol Shin, Dayeon Yun, et al. 2023. Memory-Centric Computing with SK hynix’s Domain-Specific Memory. In *2023 IEEE Hot Chips 35 Symposium (HCS)*. IEEE Computer Society, 1–26.
- [35] Yongkee Kwon, Kornijcuk Vladimir, Nahsung Kim, Woojae Shin, Jongsoon Won, Minkyu Lee, Hyunha Joo, Haerang Choi, Guhyun Kim, Byeongju An, et al. 2022. System architecture and software stack for GDDR6-AiM. In *2022 IEEE Hot Chips 34 Symposium (HCS)*. IEEE, 1–25.
- [36] Young-Cheon Kwon, Suk Han Lee, Jaehoon Lee, Sang-Hyuk Kwon, Je Min Ryu, Jong-Pil Son, O Seongil, Hak-Soo Yu, Haesuk Lee, Soo Young Kim, et al. 2021. 25.4 a 20nm 6gb function-in-memory dram, based on hbm2 with a 1.2 tflops programmable computing unit using bank-level parallelism, for machine learning applications. In *2021 IEEE International Solid-State Circuits Conference (ISSCC)*, Vol. 64. IEEE, 350–352.
- [37] Chris Lattner, Mehdi Amini, Uday Bondhugula, Albert Cohen, Andy Davis, Jacques Pienaar, River Riddle, Tatiana Shepsman, Nicolas Vasilache, and Oleksandr Zinenko. 2021. MLIR: Scaling Compiler Infrastructure for Domain Specific Computation. *2021 IEEE/ACM International Symposium on Code Generation and Optimization (CGO)* 00 (2021), 2–14. <https://doi.org/10.1109/cco51591.2021.9370308>
- [38] Dominique Lavenier, Charles Deltel, David Furodet, and Jean-François Roy. 2016. *MAPPING on UPMEM*. Ph. D. Dissertation. INRIA.
- [39] Sukhan Lee, Shin-haeng Kang, Jaehoon Lee, Hyeonsu Kim, Eojin Lee, Seungwoo Seo, Hosang Yoon, Seungwon Lee, Kyoungwan Lim, Hyunsung Shin, et al. 2021. Hardware architecture and software stack for PIM based on commercial DRAM technology: Industrial product. In *2021 ACM/IEEE 48th Annual International Symposium on Computer Architecture (ISCA)*. IEEE, 43–56.
- [40] Sukhan Lee, Shin-haeng Kang, Jaehoon Lee, Hyeonsu Kim, Eojin Lee, Seungwoo Seo, Hosang Yoon, Seungwon Lee, Kyoungwan Lim, Hyunsung Shin, Jinhyun Kim, O Seongil, Anand Iyer, David Wang, Kyomin Sohn, and Nam Sung Kim. 2021. Hardware Architecture and Software Stack for PIM Based on Commercial DRAM Technology. *2021 ACM/IEEE 48th Annual International Symposium on Computer Architecture (ISCA)* 00 (2021), 43–56. <https://doi.org/10.1109/isca52012.2021.00013>
- [41] Seongju Lee, Kyuyoung Kim, Sanghoon Oh, Joonhong Park, Gimoon Hong, Dongyoon Ka, Kyudong Hwang, Jeongje Park, Kyeongpil Kang, Jungyeon Kim, Junyeol Jeon, Nahsung Kim, Yongkee Kwon, Kornijcuk Vladimir, Woojae Shin, Jongsoon Won, Minkyu Lee, Hyunha Joo, Haerang Choi, Jaewook Lee, Donguc Ko, Younggun Jun, Keewon Cho, Ilwoong Kim, Choungki Song, Chunseok Jeong, Daehan Kwon, Jieun Jang, Il Park, Junhyun Chun, and Joohwan Cho. 2022. A 1.25V 8Gb, 16Gb/s/pin GDDR6-based Accelerator-in-Memory supporting ITFLOPS MAC Operation and Various Activation Functions for Deep-Learning Applications. *International Solid-State Circuits Conference* (2022).
- [42] Cong Li, Zhe Zhou, Size Zheng, Jiayi Zhang, Yun Liang, and Guangyu Sun. 2024. SpecPIM: Accelerating Speculative Inference on PIM-Enabled System via Architecture-Dataflow Co-Exploration. In *Proceedings of the 29th ACM International Conference on Architectural Support for Programming Languages and Operating Systems, Volume 3 (La Jolla, CA, USA) (ASPLOS ’24)*. Association for Computing Machinery, New York, NY, USA, 950–965. <https://doi.org/10.1145/3620666.3651352>
- [43] Dacheng Li*, Rulin Shao*, Anze Xie, Ying Sheng, Lianmin Zheng, Joseph E. Gonzalez, Ion Stoica, Xuezhe Ma, and Hao Zhang. 2023. How Long Can Open-Source LLMs Truly Promise on Context Length? <https://lmsys.org/blog/2023-06-29-longchat>
- [44] Bin Lin, Tao Peng, Chen Zhang, Minmin Sun, Lanbo Li, Hanyu Zhao, Wencong Xiao, Qi Xu, Xiafei Qiu, Shen Li, et al. 2024. Infinite-LLM: Efficient LLM Service for Long Context with DistAttention and Distributed KVCache. *arXiv preprint arXiv:2401.02669* (2024).
- [45] Tianyang Liu, Canwen Xu, and Julian McAuley. 2023. Repobench: Benchmarking repository-level code auto-completion systems. *arXiv preprint arXiv:2306.03091* (2023).
- [46] Ruilong Ma, Xiang Yang, Jingyu Wang, Qi Qi, Haifeng Sun, Jing Wang, Zirui Zhuang, and Jianxin Liao. 2024. HPipe: Large Language Model Pipeline Parallelism for Long Context on Heterogeneous Cost-effective Devices. In *Proceedings of the 2024 Conference of the North American Chapter of the Association for Computational Linguistics: Human Language Technologies (Volume 6: Industry Track)*, Yi Yang, Aida Davani, Avi Sil, and Anoop Kumar (Eds.). Association for Computational Linguistics, Mexico City, Mexico, 1–9. <https://doi.org/10.18653/v1/2024.naacl-industry.1>
- [47] D Manjunath, Jayakrishnan Nair, Niklas Carlsson, Edith Cohen, Philippe Robert, Christina Giannoula, Ivan Fernandez, Juan Gómez-Luna, Nectarios Koziris, Georgios Goumas, and Onur Mutlu. 2022. Towards Efficient Sparse Matrix Vector Multiplication on Real Processing-In-Memory Architectures. *Abstract Proceedings of the 2022 ACM SIGMETRICS/IFIP PERFORMANCE Joint International Conference on Measurement and Modeling of Computer Systems* (2022), 33–34. <https://doi.org/10.1145/3489048.3522661>
- [48] MosaicML. 2023. Introducing mpt-7b: A new standard for open-source, commercially usable llms. www.mosaicml.com/blog/mpt-7b
- [49] Onur Mutlu, Saugata Ghose, Juan Gómez-Luna, and Rachata Ausavarungnirun. 2020. A Modern Primer on Processing in Memory. *arXiv* (2020). <https://doi.org/10.48550/arxiv.2012.03112> [arXiv:2012.03112](https://arxiv.org/abs/2012.03112)
- [50] Deepak Narayanan, Amar Phanishayee, Kaiyu Shi, Xie Chen, and Matei Zaharia. 2021. Memory-efficient pipeline-parallel dnn training. In *International Conference on Machine Learning*. PMLR, 7937–7947.
- [51] Nvidia. 2020. Nvidia-ampere-architecture-whitepaper. <https://www.nvidia.com/content/dam/en-zz/Solutions/Data-Center/nvidia-ampere-architecture-whitepaper.pdf>
- [52] OpenAI. 2024. OpenAI o1 System Card. <https://openai.com/index/openai-o1-system-card/>. Accessed on: 2024-11-21.
- [53] OpenAI, Josh Achiam, Steven Adler, Sandhini Agarwal, Lama Ahmad, Ilge Akkaya, Florencia Leoni Aleman, Diogo Almeida, Janko Altmenschmidt, Sam Altman, Shyamal Anadkat, Red Avila, Igor Babuschkin, Suchir Balaji, Valerie Balcom, Paul Baltescu, Haoming Bao, Mohammad Bavarian, Jeff Belgum, Irwan Bello, Jake Berdine, Gabriel Bernadett-Shapiro, Christopher Berner, Lenny Bogdonoff, Oleg Boiko, Madelaine Boyd, Anna-Luisa Brakman, Greg Brockman, Tim Brooks, Miles Brundage, Kevin Button, Trevor Cai, Rosie Campbell, Andrew Cann, Brittany Carey, Chelsea Carlson, Rory Carmichael, Brooke Chan, Che Chang, Fotis Chantzis, Derek Chen, Sully Chen, Ruby Chen, Jason Chen, Mark Chen, Ben Chess, Chester Cho, Casey Chu, Hyung Won Chung, Dave Cummings, Jeremiah Currier, Yunxing Dai, Cory Decareaux, Thomas Degry, Noah Deutsch, Damien Deville, Arka Dhar, David Dohan, Steve Dowling, Sheila Dunning, Adrien Ecoffet, Atty Eleti, Tyna Eloundou, David Farhi, Liam Fedus, Niko Felix, Simón Posada Fishman, Juston Forte, Isabella Fulford, Leo Gao, Elie Georges, Christian Gibson, Vik Goel, Tarun Gogineni, Gabriel Goh, Rapha Gontijo-Lopes, Jonathan Gordon, Morgan Grafstein, Scott Gray, Ryan Greene, Joshua Gross, Shixiang Shane Gu, Yufei Guo, Chris Hallacy, Jesse Han, Jeff Harris, Yuchen He, Mike Heaton, Johannes Heidecke, Chris Hesse, Alan Hickey, Wade Hickey, Peter Hoeschele, Brandon Houghton, Kenny Hsu, Shengli Hu, Xin Hu, Joost Huizinga, Shantanu Jain, Shawn Jain, Joanne Jang, Angela Jiang, Roger Jiang, Haozhun Jin, Denny Jin, Shino Jomoto, Billie Jonn, Heewoo Jun, Tomer Kaftan, Łukasz Kaiser, Ali Kamali, Ingmar Kanitscheider, Nitish Shirish Keskar, Tabarak Khan, Logan Kilpatrick, Jong Wook Kim, Christina Kim, Yongjik Kim, Jan Hendrik Kirchner, Jamie Kiros, Matt Knight, Daniel Kokotajlo, Łukasz Kondraciuk, Andrew Kondrich, Aris Konstantinidis, Kyle Kopic, Gretchen Krueger, Vishal Kuo, Michael Lampe, Ikai Lan, Teddy Lee, Jan Leike, Jade Leung, Daniel Levy, Chak Ming Li, Rachel Lim, Molly Lin, Stephanie Lin, Mateusz Litwin, Theresa Lopez, Ryan Lowe, Patricia Lue, Anna Makanju, Kim Malfacini, Sam Manning, Todor Markov, Yaniv Markovski, Bianca Martin, Katie Mayer, Andrew Mayne, Bob McGrew, Scott Mayer McKinney, Christine McLeavey, Paul McMillan, Jake McNeil, David Medina, Aalok Mehta, Jacob Menick, Luke Metz, Andrey Mishchenko, Pamela Mishkin, Vinnie Monaco, Evan Morikawa, Daniel Mossing, Tong Mu, Mira Murati, Oleg Murk, David Mély, Ashvin Nair, Reiichiro Nakano, Rajeev Nayak, Arvind Neelakantan, Richard Ngo, Hyeonwoo Noh, Long Ouyang, Cullen O’Keefe, Jakub Pachocki, Alex Paino, Joe Palermo, Ashley Pantuliano, Giambattista Parascandolo, Joel Parish, Emy Parparita, Alex Passos, Mikhail Pavlov, Andrew Peng, Adam Perelman, Filipe de Avila Belbute Peres, Michael Petrov, Henrique Ponde de Oliveira Pinto, Michael, Pokorný, Michelle Pokrass, Vitchyr H. Pong, Tolly Powell, Alethea Power, Boris Power, Elizabeth Proehl, Raul Puri, Alec Radford, Jack Rae, Aditya Ramesh, Cameron Raymond, Francis Real, Kendra Rimbach, Carl Ross, Bob Rotsted, Henri Roussez, Nick Ryder, Mario Saltarelli, Ted Sanders, Shibani Santurkar, Girish Sastry, Heather Schmidt, David Schnurr, John Schulman, Daniel Selsam, Kyla Sheppard, Toki Sherbakov, Jessica Shieh, Sarah Shoker, Pranav Shyam, Szmon Sidor, Eric Sigler, Maddie Simens, Jordan Sitkin, Katarina Slama, Ian Sohl, Benjamin Sokolowsky, Yang Song, Natalie Staudacher, Felipe Petroski Such, Natalie Summers, Ilya Sutskever, Jie Tang, Nikolaus Tezak, Madeleine B. Thompson, Phil Tillet, Amin Tootoonchian, Elizabeth Tseng, Preston Tuggle, Nick Turley, Jerry Tworek, Juan Felipe Cerón Uribe, Andrea Vallone, Arun Vijayarvigiya, Chelsea Voss, Carroll Wainwright, Justin Jay Wang, Alvin Wang, Ben Wang, Jonathan Ward, Jason Wei, CJ Weinmann, Akila Welihinda, Peter

- Welinder, Jiayi Weng, Lilian Weng, Matt Wiethoff, Dave Willner, Clemens Winter, Samuel Wolrich, Hannah Wong, Lauren Workman, Sherwin Wu, Jeff Wu, Michael Wu, Kai Xiao, Tao Xu, Sarah Yoo, Kevin Yu, Qiming Yuan, Wojciech Zaremba, Rowan Zellers, Chong Zhang, Marvin Zhang, Shengjia Zhao, Tianhao Zheng, Juntang Zhuang, William Zhuk, and Barret Zoph. 2024. GPT-4 Technical Report. arXiv:2303.08774 [cs.CL] <https://arxiv.org/abs/2303.08774>
- [54] Jaehyun Park, Jaewan Choi, Kwanhee Kyung, Michael Jaemin Kim, Yongsuk Kwon, Nam Sung Kim, and Jung Ho Ahn. 2024. AttAcc! Unleashing the Power of PIM for Batched Transformer-based Generative Model Inference. In *Proceedings of the 29th ACM International Conference on Architectural Support for Programming Languages and Operating Systems*. 1–17.
- [55] Pratyush Patel, Esha Choukse, Chaojie Zhang, Aashaka Shah, Íñigo Goiri, Saeed Maleki, and Ricardo Bianchini. 2024. Splitwise: Efficient generative LLM inference using phase splitting. arXiv:2311.18677 [cs.AR] <https://arxiv.org/abs/2311.18677>
- [56] Saurav Pawar, SM Tonmoy, SM Zaman, Vinija Jain, Aman Chadha, and Amitava Das. 2024. The What, Why, and How of Context Length Extension Techniques in Large Language Models—A Detailed Survey. *arXiv preprint arXiv:2401.07872* (2024).
- [57] Minseok Seo, Xuan Truong Nguyen, Seok Joong Hwang, Yongkee Kwon, Guhyun Kim, Chanwook Park, Ilkon Kim, Jaehan Park, Jeongbin Kim, Woojae Shin, Jongsoon Won, Haerang Choi, Kyuyoung Kim, Daehan Kwon, Chunseok Jeong, Sangheon Lee, Yongseok Choi, Wooseok Byun, Seungcheol Baek, Hyuk-Jae Lee, and John Kim. 2024. IANUS: Integrated Accelerator based on NPU-PIM Unified Memory System. In *Proceedings of the 29th ACM International Conference on Architectural Support for Programming Languages and Operating Systems, Volume 3 (La Jolla, CA, USA) (ASPLOS '24)*. Association for Computing Machinery, New York, NY, USA, 545–560. <https://doi.org/10.1145/3620666.3651324>
- [58] Noam Shazeer. 2020. GLU Variants Improve Transformer. arXiv:2002.05202 [cs.LG]
- [59] Mohammad Shoeybi, Mostofa Patwary, Raul Puri, Patrick LeGresley, Jared Casper, and Bryan Catanzaro. 2019. Megatron-lm: Training multi-billion parameter language models using model parallelism. *arXiv preprint arXiv:1909.08053* (2019).
- [60] StableHLO. 2019. *StableHLO*. <https://github.com/openxla/stablehlo>
- [61] Gemini Team, Rohan Anil, Sebastian Borgeaud, Jean-Baptiste Alayrac, Jiahui Yu, Radu Soricut, Johan Schalkwyk, Andrew M Dai, Anja Hauth, Katie Millican, et al. 2023. Gemini: a family of highly capable multimodal models. *arXiv preprint arXiv:2312.11805* (2023).
- [62] The IREE Authors. 2019. *IREE*. <https://github.com/openxla/iree>
- [63] Hugo Touvron, Louis Martin, Kevin R. Stone, Peter Albert, Amjad Almahairi, Yasmine Babaei, Nikolay Bashlykov, Soumya Batra, Prajjwal Bhargava, Shrubti Bhosale, Daniel M. Bikel, Lukas Blecher, Cristian Cantón Ferrer, Moya Chen, Guillem Cucurull, David Esiobu, Jude Fernandes, Jeremy Fu, Wenyin Fu, Brian Fuller, Cynthia Gao, Vedanuj Goswami, Naman Goyal, Anthony S. Hartshorn, Saghar Hosseini, Rui Hou, Hakan Inan, Marcin Kardas, Viktor Kerkez, Madian Khabsa, Isabel M. Kloumann, A. V. Korenev, Punit Singh Koura, Marie-Anne Lachaux, Thibaut Lavril, Jenya Lee, Diana Liskovich, Yinghai Lu, Yuning Mao, Xavier Martinet, Todor Mihaylov, Pushkar Mishra, Igor Molybog, Yixin Nie, Andrew Poulton, Jeremy Reizenstein, Rashi Rungta, Kalyan Saladi, Alan Schelten, Ruan Silva, Eric Michael Smith, R. Subramanian, Xia Tan, Binh Tang, Ross Taylor, Adina Williams, Jian Xiang Kuan, Puxin Xu, Zhengxu Yan, Iliyan Zarov, Yuchen Zhang, Angela Fan, Melanie Kambadur, Sharan Narang, Aurelien Rodriguez, Robert Stojnic, Sergey Edunov, and Thomas Scialom. 2023. Llama 2: Open Foundation and Fine-Tuned Chat Models. *ArXiv abs/2307.09288* (2023). <https://arxiv.org/abs/2307.09288>
- [64] Ashish Vaswani, Noam Shazeer, Niki Parmar, Jakob Uszkoreit, Llion Jones, Aidan N Gomez, Lukasz Kaiser, and Illia Polosukhin. 2017. Attention is all you need. In *Advances in neural information processing systems*.
- [65] Tianyu Wang, Zhaoyan Shen, and Zili Shao. 2022. CNN Acceleration with Joint Optimization of Practical PIM and GPU on Embedded Devices. In *2022 IEEE 40th International Conference on Computer Design (ICCD)*. 377–384. <https://doi.org/10.1109/ICCD56317.2022.00062>
- [66] Xindi Wang, Mahsa Salmani, Parsa Omid, Xiangyu Ren, Mehdi Rezagholizadeh, and Armaghan Eshaghi. 2024. Beyond the Limits: A Survey of Techniques to Extend the Context Length in Large Language Models. *arXiv preprint arXiv:2402.02244* (2024).
- [67] Jason Wei, Xuezhi Wang, Dale Schuurmans, Maarten Bosma, Fei Xia, Ed Chi, Quoc V Le, Denny Zhou, et al. 2022. Chain-of-thought prompting elicits reasoning in large language models. *Advances in neural information processing systems* 35 (2022), 24824–24837.
- [68] Bingyang Wu, Shengyu Liu, Yinmin Zhong, Peng Sun, Xuanzhe Liu, and Xin Jin. 2024. LoongServe: Efficiently Serving Long-Context Large Language Models with Elastic Sequence Parallelism. In *Proceedings of the ACM SIGOPS 30th Symposium on Operating Systems Principles (Austin, TX, USA) (SOSP '24)*. Association for Computing Machinery, New York, NY, USA, 640–654. <https://doi.org/10.1145/3694715.3695948>
- [69] Yuting Wu, Ziyu Wang, and Wei D. Lu. 2024. PIM-GPT: A Hybrid Process-in-Memory Accelerator for Autoregressive Transformers. arXiv:2310.09385 [cs.AR] <https://arxiv.org/abs/2310.09385>
- [70] Nahsung Kim Yongkee Kwon, Kornijuk Vladimir et al. 2024. System architecture and software stack for GDDR6-AiM. <https://hc34.hotchips.org/assets/program/posters/hc34.SKhynix.YongkeeKwon.v03.pdf>. *Hotchips2024* (2024).
- [71] Gyeong-In Yu, Joo Seong Jeong, Geon-Woo Kim, Soojeong Kim, and Byung-Gon Chun. 2022. Orca: A Distributed Serving System for Transformer-Based Generative Models. In *16th USENIX Symposium on Operating Systems Design and Implementation (OSDI 22)*. USENIX Association, Carlsbad, CA, 521–538. <https://www.usenix.org/conference/osdi22/presentation/you>
- [72] Shulin Zeng, Jun Liu, Guohao Dai, Xinhao Yang, Tianyu Fu, Hongyi Wang, Wenheng Ma, Hanbo Sun, Shiyao Li, Zixiao Huang, Yadong Dai, Jintao Li, Zehao Wang, Ruoyu Zhang, Kairui Wen, Xuefei Ning, and Yu Wang. 2024. FlightLLM: Efficient Large Language Model Inference with a Complete Mapping Flow on FPGAs. In *Proceedings of the 2024 ACM/SIGDA International Symposium on Field Programmable Gate Arrays (Monterey, CA, USA) (FPGA '24)*. Association for Computing Machinery, New York, NY, USA, 223–234. <https://doi.org/10.1145/3626202.3637562>
- [73] Ming Zhong, Da Yin, Tao Yu, Ahmad Zaidi, Mutethia Mutuma, Rahul Jha, Ahmed Hassan Awadallah, Asli Celikyilmaz, Yang Liu, Xipeng Qiu, and Dragomir Radev. 2021. QMSum: A New Benchmark for Query-based Multi-domain Meeting Summarization. In *Proceedings of the 2021 Conference of the North American Chapter of the Association for Computational Linguistics: Human Language Technologies*, Kristina Toutanova, Anna Rumshisky, Luke Zettlemoyer, Dilek Hakkani-Tur, Iz Beltagy, Steven Bethard, Ryan Cotterell, Tanmoy Chakraborty, and Yichao Zhou (Eds.). Association for Computational Linguistics, Online, 5905–5921. <https://doi.org/10.18653/v1/2021.naacl-main.472>
- [74] Minxuan Zhou, Weihong Xu, Jaeyoung Kang, and Tajana Rosing. 2022. TransPIM: A Memory-based Acceleration via Software-Hardware Co-Design for Transformer. *2022 IEEE International Symposium on High-Performance Computer Architecture (HPCA) 00* (2022), 1071–1085. <https://doi.org/10.1109/hpca53966.2022.00082>